The Geological Society of America
Special Paper 553

Terrestrial ejecta suborbital transport and the rotating frame transform

Thomas H.S. Harris*
Retired, Lockheed Martin Space Systems, Brooklyn, New York 11231, USA

ABSTRACT

Suborbital analysis (SA) is presented here as the study of ballistics around a spherical planet. SA is the subset of orbital mechanics where the elliptic trajectory intersects Earth's surface at launch point *A* and fall point *B*, known as the *A*-to-*B* suborbital problem, both launch and fall points being vector variables. Spreadsheet tools are offered for solution to this problem, based on the preferred simplified two-body model. Although simplistic in top-level description, this problem places essential reliance on reference frame transformations. Launch conditions in the local frame of point A and rotating with Earth require conversion to the nonrotating frame for correct trajectory definition, with the reverse process required for complete solution. This application of dynamics requires diligent accounting to avoid invalid results. Historic examples are provided that lack the requisite treatment, with the appropriate set of solution equations also included. Complementary spreadsheet tools SASolver and Helix solve the *A*-to-*B* problem for loft duration from minimum through 26 h. All provided spreadsheet workbook files contain the novel three-dimensional latitude and longitude plotter GlobePlot. A global ejecta pattern data set calculated using SASolver is presented. As visualized through GlobePlot, SASolver and Helix provide solutions to different forms of the *A*-to-*B* problem, in an effort to avoid errors similar to the historic misstep examples offered as a supplement. Operating guidelines and limitations of the tools are presented along with diagrams from each step. The goal is to enable mechanically valid interdisciplinary terrestrial ejecta research through novel perspective and quality graphical tools, so others may succeed where 1960s National Aeronautics and Space Administration researchers did not.

INTRODUCTION

The governing Cold War paradigm and space-age orbital analysis (OA) has a subset called suborbital analysis (SA), wherein the trajectory ellipse intersects Earth at ascending point ***A*** and descending point ***B***, typically considered for ballistic "payload delivery" in the classified defense sector. The basic form of this problem presents the launch location at point ***A*** along with "local" launch conditions of speed and direction at that point, giving rise to the need for proper mechanical treatment. $\boldsymbol{F} = \mathrm{m}(\boldsymbol{a})$ only holds true in the nonaccelerating frame, and rotation generates an apparent acceleration field for observers in that frame. Rotating frame transformation is the key for mechanically valid

*Thomas H.S. Harris https://orcid.org/0000-0001-7948-0593

Harris, T.H.S., 2022, Terrestrial ejecta suborbital transport and the rotating frame transform, *in* Foulger, G.R., Hamilton, L.C., Jurdy, D.M., Stein, C.A., Howard, K.A., and Stein, S., eds., In the Footsteps of Warren B. Hamilton: New Ideas in Earth Science: Geological Society of America Special Paper 553, p. 271–292, https://doi.org/10.1130/2021.2553(23).

results in problems like the ***A***-to-***B*** suborbital problem, due to Earth's daily rotation. Historic 1960s and late 1970s example attempts at suborbital ejecta transport modeling, from the space and earth sciences, respectively, lacked proper treatment of this problem, with lasting effect.

Point ***A*** is fixed to Earth's surface and rotates with Earth, such that any local reference frame affixed to point ***A*** is also rotating. The locally defined launch conditions at point ***A*** must be converted to equivalent values in the nonrotating or inertial frame before dynamically correct solution is possible, according to fundamental tenants of dynamics. The model presented here performs the required reference frame conversion from local frame to nonrotating frame automatically, determines the trajectory ellipse in the nonrotating frame, resolves the loft duration or time of flight (ToF) and latitude of fall point ***B***, and finally resolves the longitude of fall point ***B***, in that order.

The necessity of this dynamical accounting invalidates results that do not properly apply the same. Straight lines drawn on flat maps fail to properly characterize ejecta transport, especially at higher ejection or "launch" speeds. Efforts to map an ejecta emplacement by assuming such linear relationships in Earth's rotational paradigm will fail as the kinetic energy (KE) of the ejecta increases, loft time or ToF increases, and Earth's rotational displacement during the increased loft time also increases to convolute the emplaced fall pattern. Speed and KE are similar but notably different descriptors, with KE always proportional to the square of scalar speed.

Ultimately, the overall scenario being considered for terrestrial ejecta transport modeling must serve as a guide for the researcher using the simplified two-body model provided here. Because partitioning of hypervelocity impacts is subject to the normal constructs of continuity of energy, mass, and momentum, these "bigger picture" concepts should be the principal guidelines while modeling terrestrial ejecta transport, both strategically and, more importantly, observationally. Astronomical partitioning involves deposition of massive energy across an unknown surface and the resulting damage to that target surface, with some damaged volume flying away, i.e., the ejecta. The precursor surface is "unknown" because it no longer exists there, having been damaged and removed by the event, and by subsequent geologic modification. Part of any reasoned ejecta transport analysis must include partitioning consideration, especially with regard to thermal alteration of the ejecta.

As a general guide from the physical science component of this effort, all processes acting upon terrestrial cosmic impact ejecta are of interest in transport modeling, ballistic or otherwise, to build cross-checking into the model and (hopefully, ideally) improve validity, applicability, utility, etc. Thermal and pressure alteration are the most important indicators for reconstructing the ejection and transport motive operators. Morphologic character is another very important indicator, ranging through all physical scales, from limit-of-detection small to unit scale of the ejecta studied, or perhaps even larger. In reconstructing the target portion from which the ejecta came, the unit scale of that rock or sediment, or even the setting scale of the overall target, may come into play. Partitioning analysis is a wide-open area for development, especially for oblique impact conditions of various character, or other factors leaving reduced or relatively subtle or otherwise convoluted damage signatures. Impact research still has plenty to learn from mother nature and the geologic record.

A simplified model for the suborbital ***A***-to-***B*** problem is presented and explained here in historic context, for contemporary application of suborbital terrestrial ejecta transport. The model ignores all atmospheric effects at the start and end of the suborbital trajectory, assuming those effects to be of lesser order than that of the orbital dynamic. This applies during reentry, when the object of interest is unboosted, as well as during the ascent phase, when overwhelming forces of planetary impact are close at hand, casting atmospheric effects aside. These are the scales for which this suborbital model is valid. This is a reasonable assumption for a geographic ejecta transport range ("ground range") of several times the atmospheric depth or more. Any shorter range may be affected significantly or substantially by the atmosphere during the non-suborbital portion of transport, i.e., if it is the major portion of transport. Unless….

For ejecta launching steeply upward at high energy, reentry and atmospheric descent may represent the lessor portion of the overall transit, even if the fall is near the launch or ejection site. Thermal and pressure alteration observations are a good guide here because of the energy required for such alteration processes. When it is devolatized and vacuum quenched, highly thermally altered ejecta should be considered "distal" no matter where it lands, according to informed observations of the laws of suborbital ballistics. We can observe the units of work required to melt versus that required to propel a unit of mineral mass, be it sediment or consolidated: The difference is stark. For the phase change from solid to liquid, the equivalent speed becomes extreme, since the melting process requires orders of magnitude more energy per unit mass than any temperature change of a few or even a few hundred degrees.

The nonlinear nature of temperature and enthalpy across phase changes gets progressively more extreme for each transition from solid to liquid to vapor to plasma. Mineral alteration of virtually any variety taking place fully in the solidus indicates orders of magnitude less energy involvement than that of the phase changes. These energy-equivalence concepts are critical for suborbital ballistic modeling exploits. "Heat" and "energy" (each a different name for the same entity, along with "work") are the masters of our universe, so where they go, we must follow, in order to reconstruct and explain what happens here on our own rocky, rotating piece of that universe. This goes for physical mechanics in general, and for suborbital ballistic ejecta studies in particular. Ejecta should therefore be considered to be "distal" or "proximal" ejecta based primarily on the state of thermal and pressure alteration as a reflection of energy level of the ejection process, and perhaps only secondarily per emplaced distance from the source when a source is known. Melted ejecta is almost certainly distal in all cases, as explained below.

Following a severe local depositional impulse from a hypervelocity impact, shock wave propagation and target mass ejection redistribute energy deposited by the impact, typically dissipating the energy from the immediate area of the impact. Average energy density in the target mass is therefore expected to decrease over time after passage of the initial shock. Possible exceptions involve channeling or constructive interference of waves reflected and/or focused by variable impedance within the target mass, a possibility with any wave propagation scenario in mechanics. Another possible exception involves energy delivered back to the target area from the local overhead via interaction with energized ejecta some time after the impact. Both of these exceptions may be more likely with target mass that is layered and/or composed of a significant or substantial volatile fraction. Neither of these exceptions are considered common in a terrestrial setting, nor are they treated in this work. We also expect the phenotypes or proxies of process energy level to be ejection speed and heat (or temperature as its indicator) of the ejecta, for naturally occurring transport of energy arising from a potential gradient (from any cause). The target-projectile mixture (with whatever projectile percentage depending on incident angle) starts out energy-supersaturated by the impulse, with excavation driven by the local energy gradient thereafter. Excavation carries away energy, reducing the remaining energy and the local energy gradient over time. We expect ejection energy proxies to decrease over time as well during excavation development, once the depositional impulse is essentially complete (i.e., once the overall system is no longer externally forced). Some basics of hypervelocity impact partitioning are available in Schultz and Gault (1990), and works referenced within.

Naturally, any trends of all emplaced ejecta from a given event should also be considered as a whole, along with specifics such as relative columnar positions of different thermally processed ejecta at a given location, etc. In any case, field observations should be a primary guide for any speculation considered using the suborbital ballistic model. This model is arguably most valid for the highest thermally processed ejecta, and perhaps less so as thermal alteration decreases. As a baseline, unmelted fragments within the same strewn field as melted ejecta may just as likely imply target mass volatile expansion or other means acting as a transport motive agent, versus implying a local source site; such factors should be considered with the overall set of observations for a given impact event. As one example, the Chicxulub impact crater provided interhemispheric transport of unmelted ejecta. Glass and Koeberl (2006) offer another example, applying proximal ejecta model methodology in the form of ejecta blanket thickness (aerial concentration) to distal ejecta known as microtektites from the mid Pleistocene, when global extinctions of benthic foraminifera peaked in every ocean basin per Hayward et al. (2012).

As a general guideline for working the ***A***-to-***B*** suborbital ejecta transport problem, increased speed or KE of ejecta at launch typically results in longer loft time. In cases where earlier ejection time in the outflow development equates to higher specific KE, greater thermal alteration, and higher ejection speed for a given differential mass of ejecta, we may expect the earlier departing ejecta to land after its later-ejected neighboring target mass. Also, heat deposition of highly oblique incidence is likely to be more spread out across the surface, having multiple concentrations, with each coming at different times during the relatively extended projectile disruption. Such an extended time scale is still relatively brief or fleeting compared to that of subsequent excavation.

Additionally, for very high-KE cases, such as the Chicxulub event, with large amounts of ejecta mass, atmospheric effects may become important for later-ejected and/or more spatially continuous portions of that mass having lower speeds, with pressurized fluid cushioning from the portion of atmosphere trapped and heated beneath lofted target mass. Circular orbital speed at low altitude is roughly 8 km/s, so any significant fraction of this speed tangentially oriented relative to Earth reduces the apparent weight of ejecta in Earth's gravity, thus reducing the subordinate pressure required to sustain loft.

With heat to deliver along its path, lofted ejecta mass can potentially travel extended distances at suborbital speed while energizing its own supporting cushion, an unpleasant concept for anyone near such a superatmospheric "pyro-mentum" current or sheet-flow scenario. This case is not appropriate for the simplified two-body suborbital model by itself; however, a modified version of this suborbital model with reduced gravity may be helpful. Lowering the gravity constant of the model as a function of fractional circular orbital speed may provide first-order insight as to the global behavior of superatmospheric "skidding" flow. Such an effort may indicate the resultant pressure rise across the regional surface beneath such flow (i.e., proportional to suspended weight/circular-orbit-speed ratio), the associated temperature when radiative effects are also considered, and the chances of spontaneous combustion and/or vapor phase transition of surface materials exposed to those conditions. Oceans may be favorable for extended skidding range due to effective steam cushioning, as with pyroclastic flows, etc. Earth is a unique case in this regard, with a majority of its surface covered by liquid or solid water.

In general, when ejecta melt or more thermally altered ejecta is found sporadically within the basal layer of a continuous blanket of less thermally altered ejecta, it indicates that suborbital transport may not have been the sole mechanism at work. In such a case, atmospheric cushioning of the blanket mass may have enabled relatively low-speed transport over long distance ranges. The complexities of such a "cushioning" scenario may involve an extended duration of energy transfer between ejecta and subordinate atmospheric gasses during transport. Nonballistic transport is not covered by the simplified two-body suborbital model, where energy is conserved per the first law of thermodynamics. In simplified two-body orbital and suborbital motion, the elliptical trajectory is defined by an exchange of potential energy with kinetic energy while their

sum remains constant. Solution definitions of the model are provided in Appendix S1.[1]

Suborbital analysis ballistic solver SASolver (Supplement 1) and graphical tool GlobePlot are provided here as Supplemental Material to study the ***A***-to-***B*** suborbital problem. Novel "all-***A***-to-***B***" solver Helix (Supplement 2), Appendix S1 equations and the user guide for the pair of spreadsheet tools (Supplement 3), and a new global ejecta fall pattern data set (Supplement 4), a significant expansion of previous work by Dobrovolskis (1981), are also provided. The goal is to enable mechanically valid suborbital modeling tools and associated graphical output to mainstream interdisciplinary researchers and for education purposes down to the high-school level, for use by all interested parties per Alvarez (1990). The simplified two-body model is as sound as its tenets are old, dating to the invention of calculus.

The ***A***-to-***B*** problem has many forms, each with unique essential constraints and techniques. Rotating frame transforms are required in every form, per the governing dynamics, to assure valid results. The details of this application and its governing dynamics are often missed or ignored, with such missteps leading to nonvalid solutions. This is especially problematic when requisite rotating frame transformations are omitted, an easy error to commit from lack of awareness, yet difficult to identify due to lack of explicit presence in the work. The science of tektites brings us two useful examples demonstrating the need for appropriate dynamical accounting in rotating frame problems.

The first example, from Chapman et al. (1962), Chapman and Larson (1963), and Chapman (1964), referred to hereafter as "Chapman," is an important take-away. The example error of omission of rotating frame transformation required over half a century to identify in the otherwise high-validity body of National Aeronautics and Space Administration (NASA) research that afforded safe return of the *Apollo* astronauts from the Moon. From the 1970s, the second example is arguably a result of the first, arising from the lack of any solution being presented to the first misstep.

Detailed understanding of solution process in the ***A***-to-***B*** problem is aided by graphics for the diverse learning process: Some learn best with words, some with equations, some with imagery. Communication through all three channels best affords learning, and so a combination is employed here. The ***A***-to-***B*** suborbital problem is intensively three dimensional (3-D), with graphics highly leveraged for the various steps of the overall exercise presented.

[1]Supplemental Material. Supplement 1: SASolver suborbital ballistic spreadsheet for the ***A***-to-***B*** suborbital problem. Supplement 2: Helix spreadsheet for variable flight times of the same ***A***-to-***B*** suborbital problem. Supplement 3: Appendix S1 followed by the spreadsheet tools user guide. Supplement 4: Global ejecta fall patters (19 files) for incremental launch conditions of azimuth, elevation, and speed, and for incremental launch location latitude. Please visit https://doi.org/10.1130/SPE.S.19310969 to access the supplemental material, and contact editing@geosociety.org with any questions.

A-TO-*B* MODEL DESCRIPTION AND METHOD

The ***A***-to-***B*** model for ejecta fall emplacement patterns on a rotating planet was developed in the nondimensional model of Dobrovolskis (1981) for application across various bodies of our solar system. This work details terrestrial application by using Earth's constants of scale, mass, and spin rate. Atmospheric effects are not considered, and model Earth is spherical. The provided spreadsheet solver tools may be generalized per Dobrovolskis (1981) for application to rotating, gravitating bodies other than Earth simply by substituting appropriate values for the aforementioned constants.

The basis for this material was originally developed within the space and planetary sciences sectors, often using the same simplified two-body model applied here. The 1950s and 1960s renditions often included additional treatments of initial ascent "boost" phase and final descent reentry phase for defense-related "payload delivery" applications. In the public sector, those publications were typically limited to inertial solutions, i.e., with inertial range or central flight angle of the inertial ellipse as the tabulated value for a given spread of launch conditions. Such solutions neglect the effects of Earth's rotation. The launch condition spread was also typically limited to that of available ballistic launch vehicle technologies of the era, which were insufficient to fully address the terrestrial ejecta paradigm, per Chapman (1964).

The current effort is to provide an easy-to-use tool with a comfortable interface and clearly defined mathematical method. The offering is tailored for use by earth science researchers and others not necessarily familiar with space science applications such as intercontinental payload delivery as developed for national defense interests. The spreadsheet is programmed and notated with references from chapter 1 of Bate, Mueller, and White (1971), hereafter "B.M.W. (1971)," chosen for its historic priority among the available references. Some SASolver graphics are dedicated to reproduce B.M.W. (1971) example diagrams automatically for any case entered. Detailed mathematical treatment is embedded in the spreadsheet tools and provided in Appendix S1, "Variable Definitions for the ***A***-to-***B*** Suborbital Problem."

A graphical representation of each spreadsheet tool layout is also included in Appendix S1, showing where each section of equations is programmed within each workbook. The four sections of equations are: (1) terrestrial constants and initial conditions, (2) inertial velocity vector components and flight path angle at launch, (3) inertial orbit variables and rotation matrices, and (4) time of flight and fall site calculation. These sections are also marked on the spreadsheet layout diagrams of each provided spreadsheet tool in Appendix S1. The ballistic calculator SASolver (Supplement 1) solves the list of variables in a column, while the "all ***A***-to-***B***" solver Helix (Supplement 2) does so in a row configuration. The rotation matrices allow simple matrix rotation of a block of 3-D positions (i.e., trajectory point set), with the trajectory point set being calculated within SASolver using the polar orbit equation in Figure 1A. SASolver allows

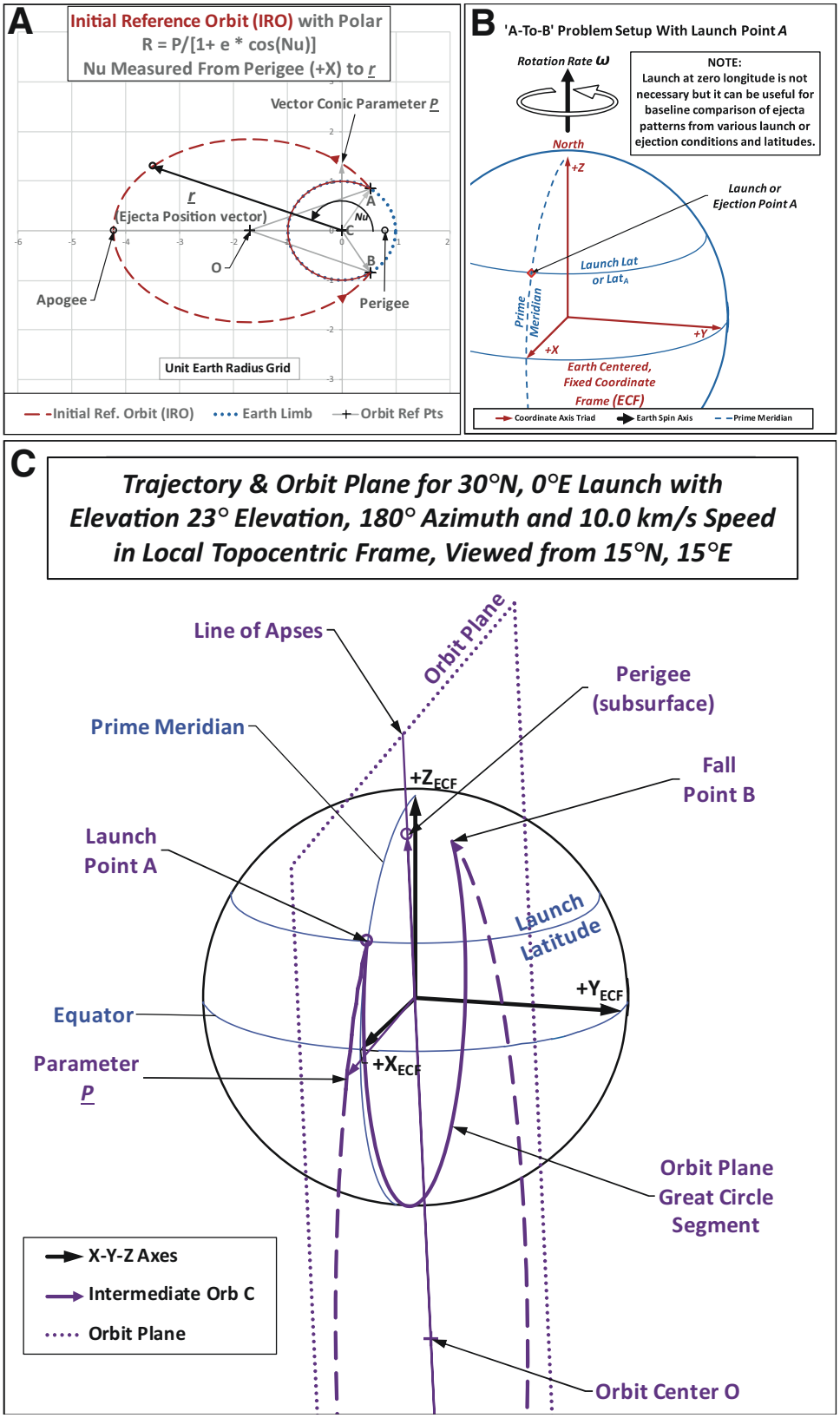

Figure 1. Stages of an example ***A***-to-***B*** solution process. (A) Conversion of the user input values from rotating to nonrotating frame allows definition of the trajectory ellipse, with associated polar equation containing eccentricity ***e*** to describe the shape of the ellipse and vector conic parameter ***P*** to establish its scale. (B) Rotating frame environment of launch, with Earth's spin rate, ω, being right-handed for the north pole. (C) Combination of the trajectory from part A applied to the launch point of part B for due south launch at low elevation and 10 km/s speed as observed in the local launch frame, which is rotating (affixed to rotating Earth). Due south locally observed launch condition does not produce a polar orbit, with observable narrow angle difference between orbit subtrack (orbit plane great circle segment) and prime meridian in the lower center of part C. Compared to unit Earth radius, $|P| > 1$ describes second-way or long-way ***A***-to-***B*** trajectories, $|P| < 1$ describes first-way or short-way suborbit trajectories, and $|P| = 1$ describes antipodal ***A***-to-***B*** point pairs.

intensive inspection of a given trajectory from every perspective. Helix allows intensive inspection of a given ***A***-to-***B*** solution set, i.e., multiple trajectories of different loft duration or ToF, all between the same points ***A*** and ***B***. The two SA utilities are complementary and offer best results when used together along with GlobePlot for visualization.

The ***A***-to-***B*** suborbital problem is extremely well suited for generating three-space trajectory graphics data, based on very few input variables, using the supplied spreadsheet tools. With intermediate rotation matrices individually identified, every step of the solution is made available, with calculated data blocks and graphics preprogrammed, in addition to the final solved state. Launch location (latitude/longitude) along with the launch condition (typically elevation, azimuth, and speed, denoted EL-AZ-VEL) provide sufficient definition to solve two angles locating fall point ***B*** where one exists. Here VEL actually stands for scalar speed to preserve the ballistics and rocketry heritage of the EL-AZ-VEL phrase, and because VEL rhymes with EL to make the order easier to learn and use. Each ***A***-to-***B*** combination has infinite solutions through a continuum of loft duration or ToF, typically having two solutions for each discrete ToF, a short way or first way and a long way or second way. These nuances dictate the need for multiple solution tools, and they make it important to understand what is going on in the model.

The ***A***-to-***B*** suborbital problem for ballistic ejecta transport is one where the launch conditions represent the impact ejection conditions applied at launch point ***A***. The ejecta ascends from Earth's surface from ***A*** along an elliptical trajectory and eventually intersects Earth's unit radius once more at point ***B*** upon descent. The launch is considered to be impulsive, with speed imparted instantaneously at point ***A***. In reality, this equates to assuming infinite acceleration, an unrealistic construct. Because the planetary impact environment is violently explosive, the impulsive launch assumption should apply reasonably well (to the first order) as long as the trajectory extends to far greater distance than the acceleration phase due to the dominant causal blast. The employed simplified two-body model uses inverse-square attraction and assumes central body mass >> orbiting particle mass.

SASolver AND HELIX SPREADSHEET TOOLS

At the top level, the state of the orbit may be determined by any five of seven variables, with the other two variables being resolvable using the model. In traditional ballistics, the launch location and condition at point ***A*** provide the requisite five values to solve for location of fall point ***B*** (lat/long), per Figure 1. For each case of known ***A*** and ***B***, an infinite set of solution trajectories exists over the continuum of ToF. If ***B*** is known, and launch conditions are assumed, then the location of point ***A*** may be solved where it exists, and the boundaries of that domain may be defined. This is the inverse or "back-solve" version of the ***A***-to-***B*** problem, or the "Chapman problem." NASA aerodynamics researcher Chapman derived reentry conditions of naturally occurring planetary impact ejecta melt that flew into space and solidified before falling back through Earth's atmosphere. Using suborbital symmetry, the reentry conditions may be assumed as symmetric or equivalent, to the first order, to the conditions of launch, in terms of speed and angle from horizontal. Details of back-solve strategy, methodology, error analysis, automated programming, or other application are left to later work, with hints of the back-solve process offered in the Results section here. The focus is on the workings of the ***A***-to-***B*** SA model.

Bate et al. (1971), Dobrovolskis' (1981) nondimensional treatment, and further expansion by Alvarez (1996) each offer useful background for derivation and application tips, tricks, and traps. The reader is encouraged to seek out these works and study the transport regime evolution through the range of launch KE values. The simplicity of the ellipse-intersecting-the-circle diagram in the above references and Figure 1A is deceptive. Governing quantities of specific mechanical energy and specific angular momentum are conserved during suborbital flight, but the potential field is nonlinear across space due to gravity's inverse-square attraction. The zero mechanical energy datum is chosen at infinite distance, making all orbital values negative, i.e., displaced or "captured" within Earth's potential well. The references and Supplement 4 of this work demonstrate the highly nonlinear advance of suborbital ejecta fall pattern convolution with increasing launch KE, a critical factor in terrestrial ejecta transport modeling that is due to the effect of Earth's rotation.

The term "ground range" implies distance measured across Earth's surface in the rotating frame. The term "inertial range" is typically used to describe the central flight angle measured from the ends of the ***A***-to-***B*** chord through Earth's center, in the inertially fixed plane of the trajectory ellipse of the governing simplified two-body model. Both phrases are self-explanatory in terms of their related property, which is helpful. The two range quantities typically diverge as loft duration blossoms geometrically with increasing launch KE, and so does westerly displacement of ejecta due to Earth's rotation beneath the fixed orbit plane as a result. Treatments from before the 1970s tended to solve for inertial range only, considering only the shorter loft duration afforded by available launch vehicles of the epoch and their limited available change in velocity (ΔV) compared to Earth's escape speed. VEL is used in the aerospace tradition for scalar launch condition of speed (i.e., EL-AZ-VEL), although the formal definition of velocity is a vector with magnitude (a scalar) and 3-D direction (defined by at least two or more additional scalars).

The individual sheets of all provided tools are protected ("locked") against user alteration. All required input cells are already unlocked using the Format menu of the Home ribbon in Microsoft Excel, and there are no protections at the workbook or file level. There are no passwords in the as-provided state of the tools, and any sheet may be unlocked or "unprotected" within the Review ribbon of Microsoft Excel. This is done at the user's assumption of all risk to the tools and the platform being used, and it is not advised for those not extremely well versed in the Excel operating environment. Further, once an "unprotect" action

is taken, the sheet may be locked or protected once more. The Protect Sheet menu has provision for password-protection, for which the user also assumes full risk. Microsoft clearly states that they cannot help recover a lost or forgotten password. If a user wants to experiment with these options for whatever the reason, it is far better to do so on an experimental spreadsheet file of no consequence, in case of file corruption or other problems arising from ill-fated efforts. The best practice is to save an unchanged "safety" copy to one or more dedicated folders or memory cards, etc., after download.

Although each sheet of these tools may be unlocked or "unprotected" within the Review ribbon of Microsoft Excel, a far better strategy is to leave all of the provided (and heavily interlinked, carefully arranged, etc.) sheets as-is and copy any sheet of interest for experimental purposes, adding it to the existing workbook. This is permitted by Excel even when a sheet is locked, producing a locked copy that is not password-protected and easily unlocked within the Review ribbon of Excel. Again, one or more unaltered "safety" copies kept in their own folders or on their own external memory device of choosing is best practice.

After the graphical setup to study each case is considered, it is best to leave each case-specific file as-organized after those user efforts, especially before full proficiency is developed by the user. The original files are free to download regardless of repetitive use and only take a few megabytes of storage, so there is little need to erase old work to make room for new. On the contrary, results that are perplexing when they first appear are sometimes the most important results for the overall learning process. They should always be saved, for the benefit of user experience, but also for the possibility of publishing. Much of the work performed with these new tools may be new or original research, so record keeping is important.

SASolver—Supplement 1

With the launch state defined by launch condition and launch location, the trajectory ellipse may be solved to determine the ToF, with the shape (eccentricity) and size (semi-major axis) of the trajectory ellipse determining the latitude of the fall point ***B***, and finally the associated longitude of point ***B***. Figure 1 depicts an example launch azimuth due south from the Northern Hemisphere at 10 km/s and low elevation, with polar equation for the trajectory ellipse (Fig. 1A). Launch angles and speed are as observed in the local launch frame, affixed to and rotating with Earth at point ***A***. Figure 1B shows the rotating "launch pad" Earth, with an example launch point at zero longitude and launch latitude Lat_A for reference. The rotating Earth provides additional eastward "throw" upon all ejecta being launched, as seen relative to the fixed distant stars or nonrotating frame, adding to eastward launch and detracting speed from westward launch, or simply perturbing otherwise polar launch directions to the north or south. The resultant orbit plane is not parallel to Earth's N-S axis, as seen by the angle between the prime meridian and the orbit plane great circle in Figure 1C. For a true polar orbit plane, the launch has to tend slightly west of north or south to nullify this eastward throw tendency caused by Earth's rotation. An impulsive launch from the surface requires an additional tangential impulse to achieve continuous orbit. Impulsive launch alone yields either suborbital or escape trajectories. Frames of Figure 1 are from the embedded graphical series of SASolver, with sheet layout and coded equations presented in Appendix S1 (Appendix S1 is in Supplement 3, along with the user guide for SASolver and Helix [see footnote 1]).

Helix—Supplement 2

Solving for ***B*** given the set of {***A*** and launch conditions at ***A***} is not always the preferred format to compute solutions of the ***A***-to-***B*** suborbital problem. Sometimes, we wish to know all possible solutions for a known ***A***-to-***B*** pair, for loft duration or ToF up to some value such as 24 or 26 h, for example. When studying emplaced ejecta from a known or proposed source, these "all ***A***-to-***B***" solutions are helpful. Figure 2 demonstrates a primary concept of SA: Variable launch conditions are required at ***A*** to reach ***B*** over different loft durations. The location of point ***A*** may be considered as fixed in nonrotating space once defined by the moment of launch, with the nonrotating frame parallel in orientation to the rotating frame at that moment. Figure 2A is in the no-rotating frame, with features of the rotating Earth undefined except for latitudes. Fall point ***B*** marches in a circle with Earth's rotation during loft.

Helix solution methodology uses Goal Seek from the Tools menu to reduce a ToF error to zero by varying eccentricity. This is not sufficient by itself to define a trajectory, but the known ***A*** and ***B*** locations combined with the preassigned ToF also define a secant chord length of Earth's sphere for scaling. The scaling condition allows resolution of semimajor axis ***a*** along with ***e***, and subsequently the rest of the orbit definition per the solution equations of Appendix S1. When new locations for ***A*** and/or ***B*** are entered, the input-output (I/O) front page of Helix shows a red "ToF ERR" notice in the output section until the "Solve" button is activated to run the automated Goal Seek routine. It will resolve over 100 solutions within a few 10s of seconds on contemporary laptop/desktop processors, with the red "TOF ERR" notice vanishing for correctly solved rows per Appendix S1, page 9.

No solution exists for the governing equations below some minimum ToF, with those rows of the I/O sheet remaining absent of data in the Helix I/O page, while the "TOF ERR" notice remains. This is not a problem and may be ignored. Page 9 of Appendix S1 shows the status of first-way and poles solutions resolved, but second-way solutions not yet resolved. The included Goal Seek solver routine may have trouble with certain orbits, in which case, an iteration limit will send it to the next row, leaving an error message on the front page for that row. The iteration limit is adjustable in the Calculation dialog/selection box from Excel Preferences. The "TOF ERR" threshold is 10^{-4} s, equating to a worst-case longitude error of <1 m (46.5 cm) at the equator, or less for all nonzero latitudes. This precision far exceeds accuracy of the simplified model employed, or terminal effects

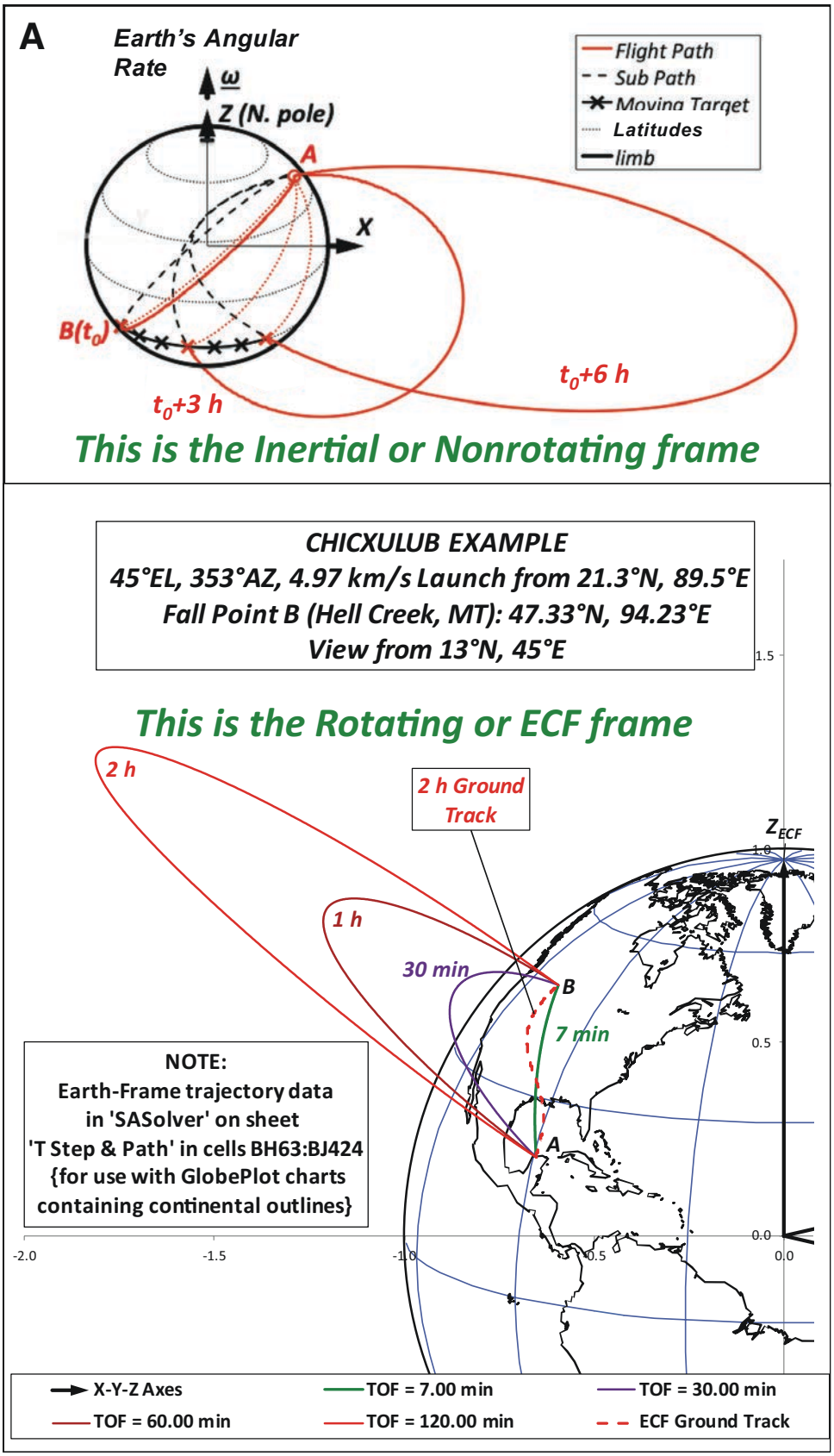

Figure 2. (A) At arbitrary time t_0, the ***A***-to-***B*** trajectory or path is at nearly zero launch elevation, a surface-hugging solution (i.e., near-minimum possible time of flight [ToF]). ***A***-to-***B*** solutions of progressively longer ToF (t_0 + 3 and t_0 + 6) show progressively higher apogee and higher launch elevation above local horizontal. (B) Same concept pictured in Earth's rotating or "Earth-centered, Earth-fixed" (ECF) frame, with continental outlines to highlight that frame. EL—elevation; AZ—azimuth. The Chicxulub example is loosely applied, with contemporary continental layout and Hell Creek, Montana (MT), as fall point ***B***. Figure clearly depicts the difference between rotating and nonrotating frames, and how the results look different between the two frames. It is marked as such in bold for good reason.

of blast thrust or atmospheric drag at launch or fall respectively. To address rows remaining above that value that still show the red TOF ERR message after solving with the buttons, the user may enter various initial eccentricity values in the appropriate row of column AX on the HelixSolver sheet in an effort to induce Goal Seek convergence. The appropriate domain is between zero and unity exclusive, with a good first-try value being 0.5 and a good second-try value being the average of the two adjacent solved eccentricity values for a TOF ERR remaining in an isolated row. Those row numbers are listed next to each solution on the I/O or front page of Helix, and eccentricity values in column AX of the HelixSolver sheet are not locked. Solving the wrong row again does not hurt, but it does waste time. The solve buttons are safe and effective.

At arbitrary time t_0 in Figure 2A, the ***A***-to-***B*** trajectory or path is at nearly zero launch elevation, a surface-hugging solution (i.e., near-minimum possible ToF). ***A***-to-***B*** solutions of progressively longer ToF (t_0 + 3 and t_0 + 6) show progressively higher apogee and higher launch elevation above local horizontal. Figure 2B is the same concept pictured in Earth's rotating or "Earth-centered, Earth-fixed" (ECF) frame, with continental outlines to highlight that frame. The Chicxulub example is loosely applied in Figure 2B, with contemporary continental layout and Hell Creek, Montana, as fall point ***B***. Defining ***A*** and ***B*** within spreadsheet Helix allows resolution of launch condition variation at ***A*** versus ToF for all cases reaching ***B***. This is accomplished by using the provided latitudes and relative longitudes of ***A*** and ***B***, and leveraging the known inverse square law of gravity. The "all ***A***-to-***B***" solution form provided by Helix helps when investigating observations of melted and unmelted ejecta from the same event found emplaced at the same distal location ***B***, or whenever both ***A*** and ***B*** are known. Figure 2 clearly depicts the difference between rotating and nonrotating frames, and how the results look different between the two frames. It is marked as such in bold for good reason.

The geometry of stationary point ***A*** and circular-gyrating point ***B*** depicted in the inertial frame per Figure 2A suggests the simple 3-D definition for time-varying ***A***-to-***B*** inertial chord length and central flight angle of that chord, per Figure 3 in the inertial or nonrotating frame, where time increases from left to right, and the slope of the diagonal line represents circular orbit at zero altitude (4.261°/min or 360° every ~5069.35 s), the minimum possible ToF between ***A*** and ***B***. Figure 3A depicts first- and second-way central flight angle time variation over 26 h, while Figure 3B expands the short ToF domain of Figure 3A to illustrate the minimum ToF envelope (diagonal line) and first- and second-way intersections with same (lower left and upper right of Figure 3B, respectively). The Figure 3 antipodal line is 180° central flight angle.

Helix solves the "all ***A***-to-***B***" problem (all ToF solutions for any ***A***-to-***B*** pair) by resolving points along that continuous solution set. The solution points are spaced at preselected ToF values to allow accurate representation for various universally common features among the global set of possible ***A***-to-***B*** suborbital solutions. The spreadsheet applies the same equation set as SASolver across 67 spreadsheet columns. Each row in Helix is a different ToF solution, and the Goal Seek function (Tools menu) must be run for each row (each discrete ToF) to resolve the eccentricity ***e***. An eccentricity value allows resolution of subsequent trajectory attributes including semimajor axis, specific mechanical energy, specific angular momentum (both constants), and launch conditions at point ***A***. The latter are defined in the local-topocentric rotating frame, i.e., per the artillery convention (and later for rocketry) of elevation, azimuth, and speed observed onsite.

By recording the execution of the Goal Seek operation using Macro (also in Tools menu), this recorded bit of code may then be embedded in a loop that steps through each ToF row in Helix, with start/stop of from/to row numbers for the programmed block of spreadsheet rows. This makes automated solution simple to execute after each new pair of points is entered, and solver buttons are available on the front page or I/O page of Helix. The same block of solver equations in Helix may be repeated for each additional fall point ***B***, a powerful technique for comparing the launch condition variation at a given point ***A*** required to reach multiple different points ***B***. This is a key strategy to find patterns in ballistic ejecta transport analysis, as demonstrated in the Results section.

The multiple fall point comparison strategy is useful for consideration of possible partitioning and outflow trends at point ***A***, and for relation to any observed structural alteration at point ***A*** as possible remnants of such partitioning. In pursuit of suborbital studies afforded by these tools, "imprint matching" is finding the ejecta pattern or KE distribution trend at point ***A*** as implied by suborbital analysis of the emplaced fall pattern (i.e., the set of all known points ***B***), to match observed structural imprinting on the ground at point ***A***. Imprint matching is guided by field observations of known ejecta and its various attributes (i.e., distribution, degree of pressure and temperature alteration, etc.) in the attempt to match those attributes imprinted upon the ejecta with observed attributes imprinted at the target or ejecta source (damage, deformation, alteration, etc.).

After Figure 3 is generated within Helix (Supplement 2), the solved parameters of various first-way and second-way suborbital trajectories may be examined for a limited set of discrete ToF values. This is helpful to visualize possibilities for a given ***A***-to-***B*** pair. Figure 4 depicts this portrait of diverse solutions with ToF on the left margin of each frame. Second-way solutions do not exist below some minimum ToF (per Fig. 3), and they are shown in Figure 4 in green where they do exist. Figure 4 is read top-to-bottom left column and then right column, for ever-increasing ToF.

All first-way and second-way suborbital solution results of Helix (Supplement 2) are also examined through their full ToF domain for any specific ***A***-to-***B*** pair as depicted in Figure 5. This "all ***A***-to-***B***" solution format is useful for comparing multiple fall points from the same source for indications of possible jetting scenarios, where all ejected mass could have come through a narrow window of launch elevation (EL) and launch azimuth

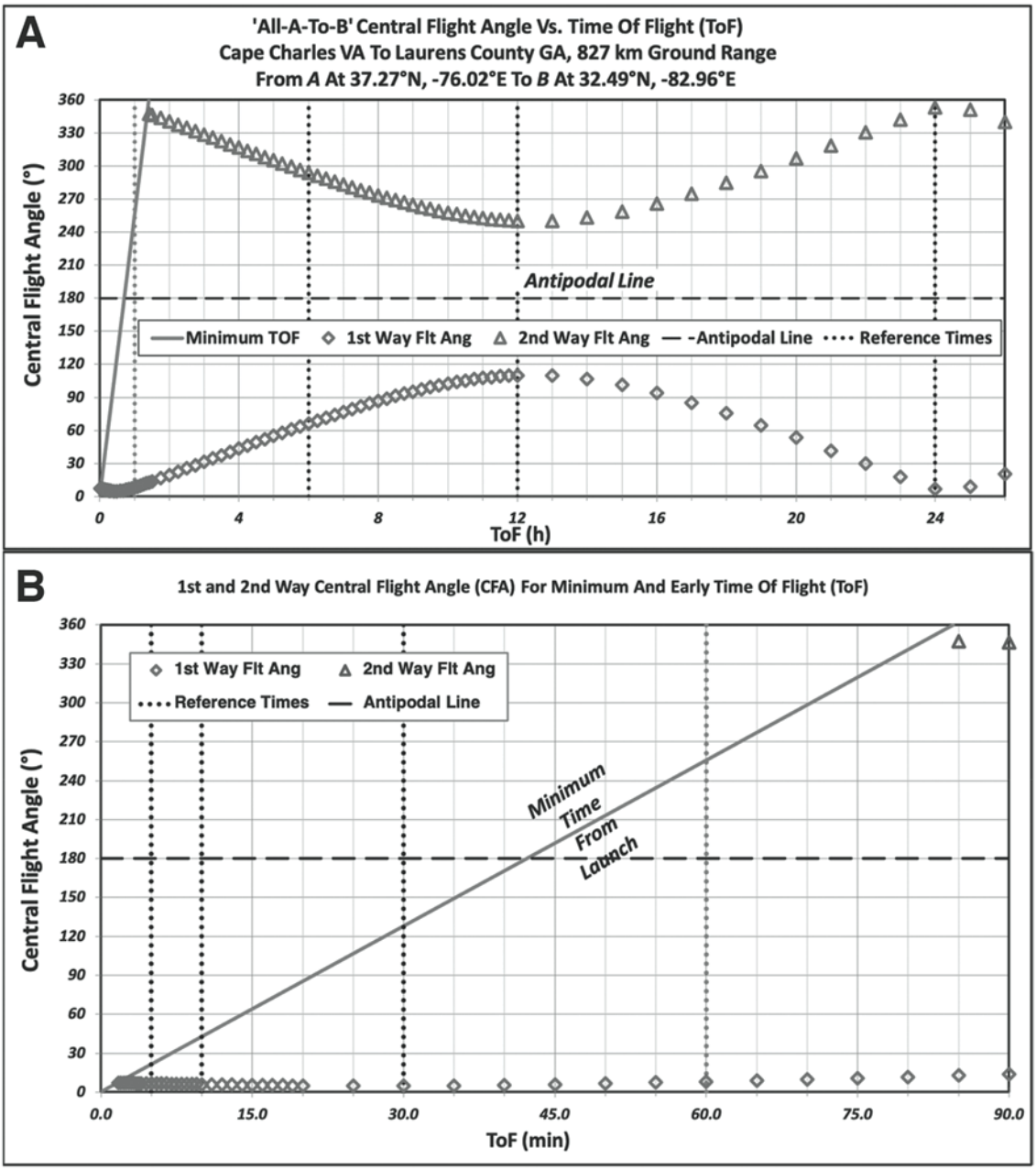

Figure 3. Plot depicting the inertial or nonrotating frame, where time increases from left to right, and the slope of the diagonal line represents circular orbit at zero altitude (4.261°/min or 360° every ~5069.35 s), the minimum possible time of flight (ToF) between ***A*** and ***B***. (A) First- and second-way central flight angle time variation over 26 h. VA—Virginia; GA—Georgia. (B) Expansion of the short ToF domain of part A to illustrate the minimum ToF envelope (diagonal line) and first- and second-way intersections with same (lower -left and upper-right part of Figure 3B, respectively). The antipodal line is 180° central flight angle.

Figure 4. Portrait of diverse solutions for the Chesapeake impact at Cape Charles, Virginia, with time of flight (ToF) on the left margin of each frame. Any ***A***-to-***B*** suborbital problem typically has two solutions for a given ToF, the first-way or short-way and the second-way or long-way solution. Second-way solutions do not exist below some minimum ToF (per Fig. 3) and are shown here in green where they do exist. Figure is read top-to-bottom left column and then right column, for ever-increasing ToF. EL—elevation; AZ—azimuth. The first two frames have nearly equal flight times of roughly 2 min and consequently their central flight angles are the same, while their launch speeds differ by more than a factor of 2 (6.901 km/s vs. 3.090 km/s) at different launch elevations and nearly the same launch azimuth. This scenario arises from a fall site located west of the launch site, similar to the case with Chicxulub impact ejecta reaching the Tanis site of contemporary SW North Dakota.

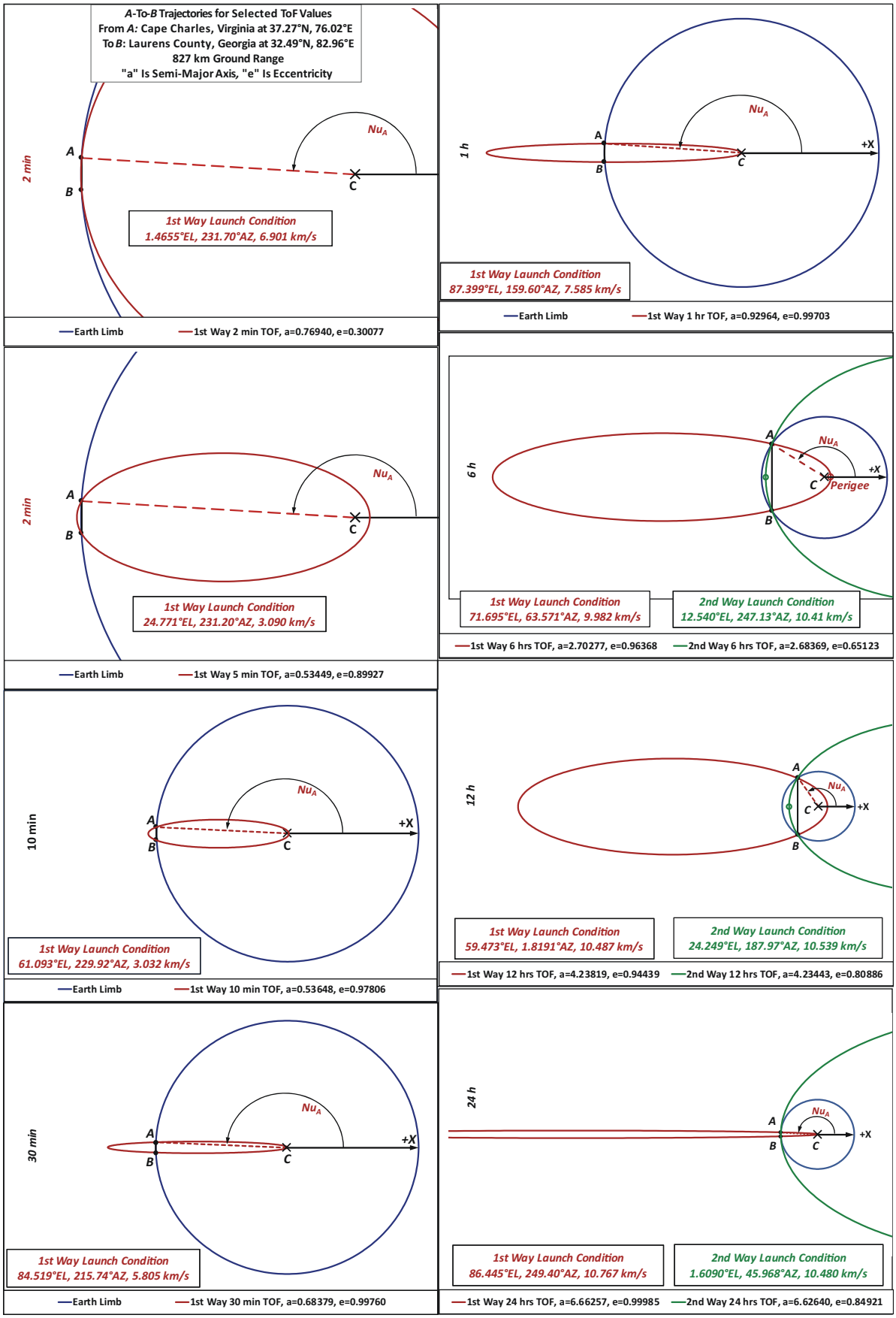

Figure 4.

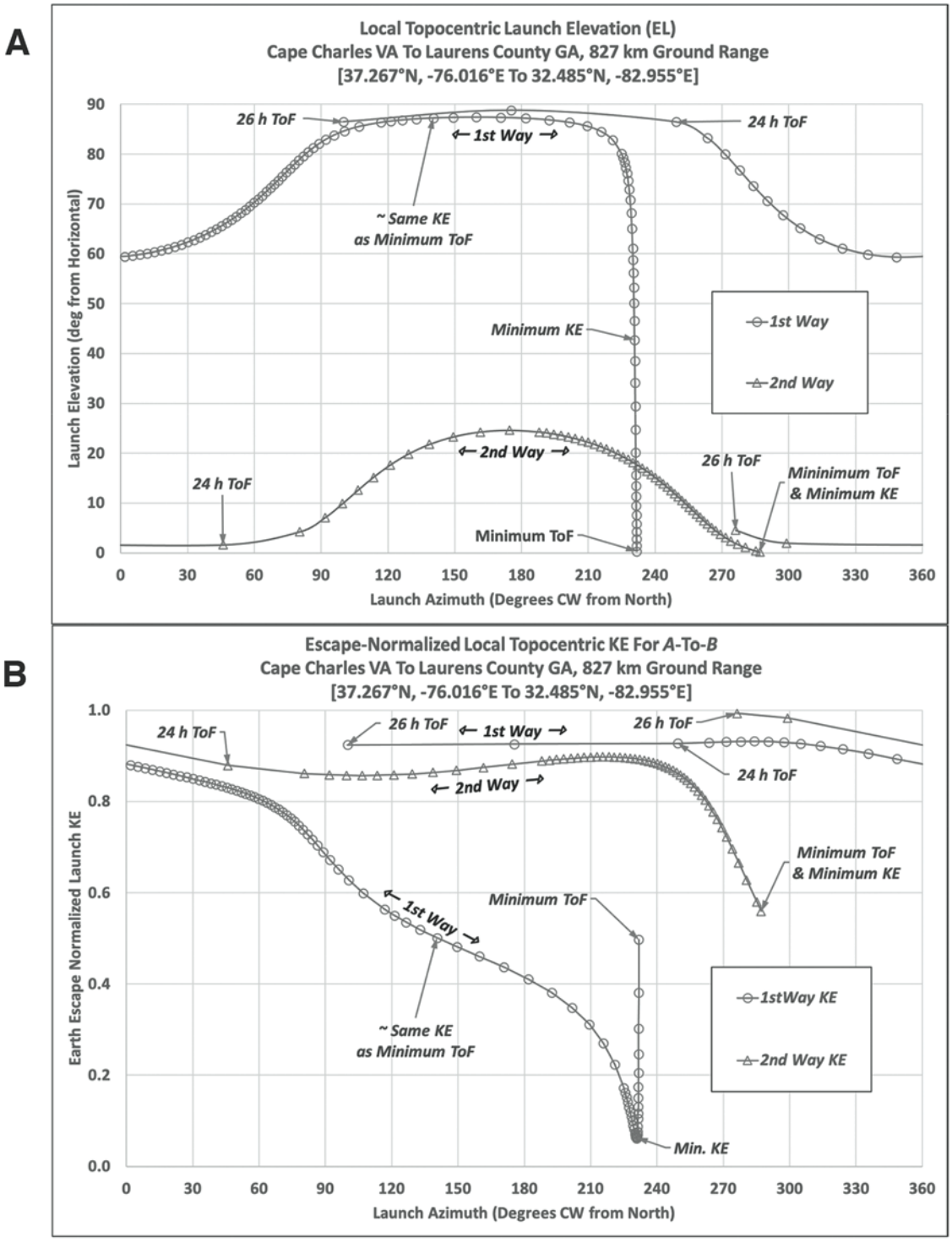

Figure 5. (A–B) Required launch elevation (EL) and launch kinetic energy (KE), respectively, depicted for the local or rotating launch frame. All first-way and second-way suborbital solution results from Helix are also examined through their full time of flight (ToF) domain for any specific ***A***-to-***B*** pair as depicted. This "all ***A***-to-***B***" solution format is useful for comparing multiple fall points from the same source for indications of possible jetting scenarios, where all ejected mass could have come through a narrow window of EL and launch azimuth (AZ) or a "small spot of the sky." While the 2nd way solutions have coincident minimum ToF and KE points, the 1st way minimum ToF and minimum KE solutions are markedly different in both launch elevation and KE. Inverse square gravitational attraction and Earth's rotating frame may produce counterintuitive results. VA—Virginia; GA—Georgia; CW—clockwise.

(AZ) or a "small spot of the sky." For the North American tektite example (Laurens County georgiaite), Figures 5A and 5B depict required launch EL and launch KE, respectively. Outflow trends from the Chesapeake impact structure centered at Cape Charles may be considered by removing the second-way curves from Figure 5 and adding solutions for bediasites and other North American tektite and microtektite fall sites, an exercise for later work (see Results for hints of what this may look like).

The character of the EL and KE versus AZ plots changes with ground distance between ***A*** and ***B***. Short ***A***-to-***B*** range is easily traversed with far lower KE by the first-way trajectories, while more distal or nearly antipodal ***A***-to-***B*** pairs show more similar first- and second-way KE requirements to reach ***B*** from ***A***. The EL, AZ, and KE values of these diagrams are referenced in the local launch frame at point ***A***, which is a rotating frame. Technically, the absolute or inertial values should be used in order to avoid required assumptions regarding the time scale of decoupling of ejecta flow from the rotating target (i.e., by assuming instantaneous complete decoupling of ejecta outflow from the rotating target frame). The two depictions are nearly identical graphically for this format. The local frame is most useful for ejecta flow characterization, for a number of reasons beyond the current scope. Target frame and inertial frame are both of utility for these comparisons.

In more detailed analysis, the time scale of the ejection impulse relative to Earth's spin rate is of interest for such coupling considerations. Ultimately, the ejecta moves independently of the frame we use to consider such motions, not subject to our conceptions of whatever construct is required. These dynamics details and assumptions are important to delineate everywhere in the process for clarity, however. Reference frame clarification is definitely an important consideration in each and every modeling choice, both when conducting and when reporting on SA work. How we choose to present findings from these tools should be guided by a sense of best-practice standards for consistent comparison of results between workers. This effort provides as many options as possible for that effort, limited by what is practical for the Excel environment.

A-to-*B* Suborbital Analysis (SA) Model: This Is Science…

Suborbital analysis is still in its infancy compared to the unique and diverse comparative potential it offers when applied to terrestrial ballistic ejecta transport. The convolution of ejecta fall patterns with increasing launch KE makes the topic of large-event ejecta transport analysis literally its own specialty. However, SA actually has the same peculiarities that fascinate kids with artillery games or spinning playground merry-go-rounds when you try to throw a ball from them. Ultimately, this is all about the world we live in, which literally surrounds our everyday existence.

Not only do we live on the surface of a big rocky wet mass that flies through space, but it also happens to be rotating, adding to the already complicated circumstances that arise when foreign projectiles collide with Earth. The infant science of SA applied to terrestrial ejecta transport can look like whatever we want it to or whatever we need it to. The work presented here follows the solution path while generating all of the diagnostics required to fully understand that path. We should let the choices behind future presentation standards be guided by the information contained in the results, so that it can best tell its own story. This is science. We measure. We compare. Tools are helpful here, especially when it comes to "rocket science."

RESULTS

The ***A***-to-***B*** model for ejecta fall emplacement patterns on a rotating planet allows calculation of global ejecta coverage for any case. The two primary spreadsheet workbook tools SASolver and Helix are contained in Supplements 1 and 2, respectively (see footnote 1). Supplement 3 contains Appendix S1 and the user guide for the pair of spreadsheet tools. A set of ejecta patterns for 5° incremental launch latitude from the equator to pole is offered as Supplement 4, consisting of 19 spreadsheet workbook files for 0° through 90° latitude at 5° increments, with solutions for south latitude easily available by reversing the latitude sign of the Northern Hemisphere results. The fall pattern data set is in identically formatted workbooks for 5° EL increments, 30° AZ increments, and 1% escape KE increments. Each workbook has 19 data spreadsheets for 2°, 88°, and 5° through 85° elevation in 5° increments.

This format is similar to that of Dobrovolskis (1981) but for the terrestrial paradigm only, expanded in resolution for launch latitudes and launch elevation, although without Dobrovolskis' rings (constant KE, full 360° launch AZ). SASolver may also be used to generate equivalent global ejecta pattern data for any discrete source latitude of point ***A***, for research of known or suspected impact structures in the field, instead of interpolating the 5° incremental latitude results.

Images from the Solution Method

The above spreadsheet tool section provided example results from intermediate steps of the solution method. Each step of the solution method is important for understanding the workings of the simplified two-body model, and for understanding each particular case being examined. Thus, the previous plots demonstrate important relationships of suborbital ***A***-to-***B*** transport in Earth's rotational environment, and they are as important, if not more so, as any single ejecta fall pattern that can be generated by the spreadsheets. Additional results offer further insight into this unique problem. All globe plots in this work are a native product of the presented tools.

Figure 6A, adapted from Alvarez (1996, fig. 4), depicts the nonlinear convolution of terrestrial ejecta fall patterns at higher launch KE. The seemingly simple, east-west symmetric launch conditions of Figure 6A produce asymmetric results as viewed in Earth's rotating frame. Rotation complicates things. That is why

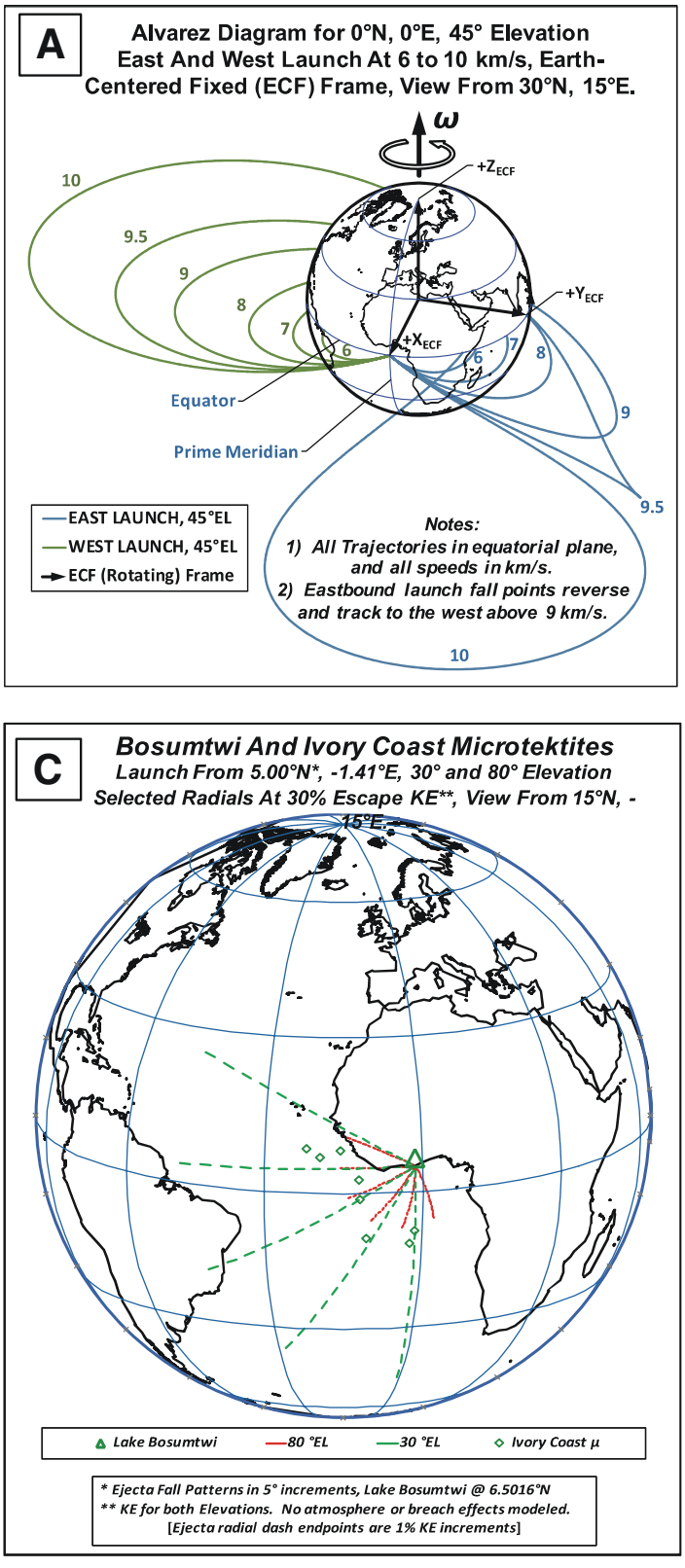

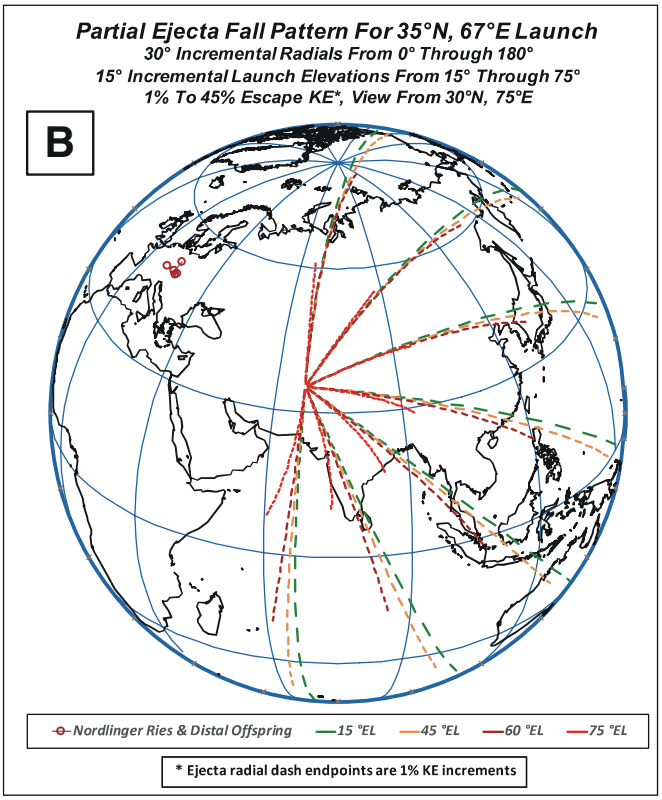

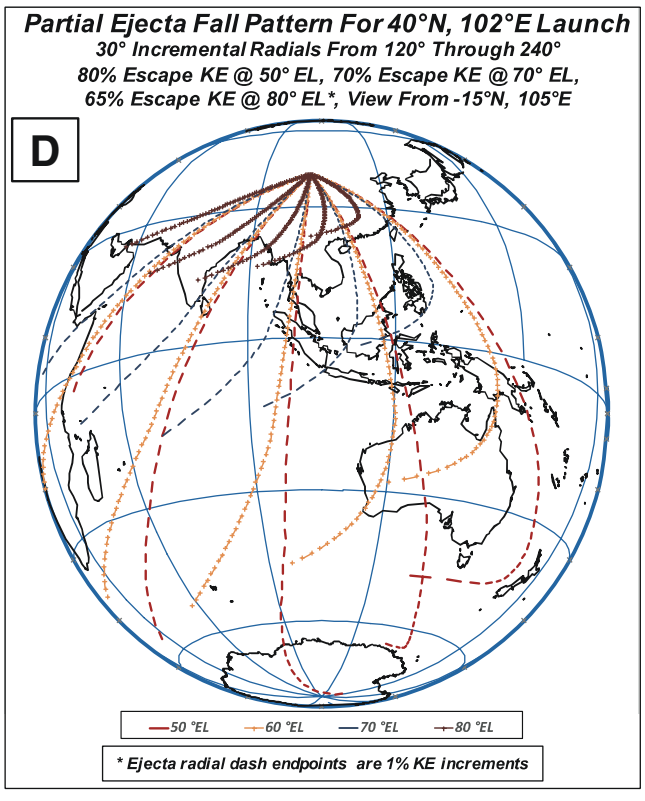

Figure 6.

Figure 6. (A) Diagram depicting the nonlinear convolution of terrestrial ejecta fall patterns at higher launch kinetic energy (KE) (adapted from Alvarez, 1996, fig. 4). Seemingly simple, east-west symmetric launch conditions in part A produce asymmetric results as viewed in Earth's rotating frame. (B) Diagram depicting filtered data from the 35° latitude–sourced ejecta fall pattern file "Supp4_35Lat&GlobeV5" (see text footnote 1), with character of the radials varying with launch elevation (EL). (C) Diagram depicting the Ivory Coast strewn field and its source, the Lake Bosumtwi impact structure. The lake is just north of 6°N latitude, so the 5° latitude fall pattern data set is used as an approximation. (D) Diagram depicting a fall pattern from North China blanketing the Indian Ocean Basin, SE Asia, the Philippines and Indonesia, Australia, Antarctica, Madagascar, and the SE African continental landmass. The south pole is reached by the 50° elevation (EL) and 180° azimuth (AZ) ejecta fall radial near the end of its 80% escape KE extension, with less energetic ejecta falling from steeper ejection angles across progressively more northerly regions of the resulting strewn field. The arcuate radials are arranged like rows of tines on a lawn rake, looking far more like the observed subfamily distribution arcs of the Australasian tektite strewn field than any lunar crater rays of Stauffer (1978) could ever reproduce.

rotating frame transformations are necessary to maintain mechanical validity of results when considering such problems. Failure to correctly apply this form of dynamical accounting means failure to correctly solve the rotating frame problem. Figure 6A sends this message home, looking like a bug's wings after a windshield encounter. Inverse square attraction combined with a rotating frame requires detailed dynamical accounting for success.

Figure 6B depicts some data from the 35° latitude–sourced ejecta fall pattern file "Supp4_35Lat&GlobeV5" (see footnote 1) for a random midcontinental longitude, azimuths 0° through 180°, and various ELs plotted from 0 to 45% Earth's escape KE, i.e., slightly less than Earth's minimum circular orbital KE of ~51% escape KE. The low EL radials cover much more distance along nearly great circle pathways, while the high EL fall pattern is much more compact and quickly diverges from great circle paths, as best shown by the 180° azimuth–75° EL radial (red) quickly curving west as it advances south from the source or launch point ***A***. All cropping of the presented ejecta fall pattern was performed on each individual data sheet for each incremental EL, as displayed with included GlobePlot version 5, a "detailed" Excel chart.

Figure 6C depicts the Ivory Coast strewn field and its source, the Lake Bosumtwi impact structure. The lake is just north of 6°N latitude, so the 5° latitude fall pattern data set is used as an approximation. Two different LEs of 30° and 80° above horizontal are used with 30% escape KE or ~6.12 km/s launch speed for selected radials to cover the strewn field from its source. In comparison, minimum circular orbital speed is roughly 8 km/s or 51% of Earth's escape KE, and unit escape speed is ~11.175 km/s. The cropping of KE and the limited selection of radial azimuths and of elevation angles are (again) simply applied using filters on the individual fall pattern data sheets for each elevation. Custom view angles with all data rotated to view are afforded with the GlobePlot utility nested within each spreadsheet tool. Data point triads have one dimension out of the page, and this value is used in filtering to remove Earth surface features on the far side of the pictured globe. This setup allows efficient manipulation of the vast ejecta fall pattern data using a common interface between the many fall pattern files of Supplement 4, as well as in the SASolver and Helix spreadsheet tools of Supplements 1 and 2, respectively. Figure 6C pictured radials are 180°, 210°, 240°, 270°, and 300°. The high EL (red) radials also include 150° AZ, with presented azimuthal spreads sufficient to populate the known seafloor fall locations. This is a simple first look to see what angles and speeds go where on the globe.

Figure 6D depicts a 40° latitude-source fall pattern for radials from 120° through 240° AZ, 50° through 80° EL at 10° increments, and 1% escape KE increments (where each dash endpoint of the dashed fall radials is 1% escape KE). This presentation of 40° latitude-sourced fall pattern data includes 5% less KE for every 10° higher launch elevation angle, a weakening ejection speed as ejection elevation increases, per an oblique impact scenario. The fall pattern from North China blankets the Indian Ocean Basin, SE Asia, the Philippines and Indonesia, Australia, Antarctica, Madagascar, and the SE African continental landmass. The south pole is reached by the 50°EL–180°AZ ejecta fall radial near the end of its 80% escape KE extension, with less energetic ejecta falling from steeper ejection angles across progressively more northerly regions of the resulting strewn field. The arcuate radials are arranged like rows of tines on a lawn rake, looking far more like the observed subfamily distribution arcs of the Australasian tektite strewn field than any lunar crater rays that Stauffer (1978) could ever reproduce. The Moon simply does not have sufficient spin compared to Earth, making it a poor proxy for use in terrestrial ejecta transport modeling due to lack of dynamic similitude.

Compare Figure 6D, depicting 65% to 80% escape KE at launch, versus adjacent Figure 6C, at only 30% escape KE. The presence or absence of arcuate dispersion and "fold-back" of ejecta fall radials is striking. These are just some of the issues lurking within the paradigm of larger-scale impacts in the terrestrial setting. The patterns have a complexity not intuitive to those uninitiated in suborbital ballistics of higher KE.

Global Ejecta Fall Patterns—Supplement 4

The SASolver output and associated GlobePlot viewer utility are assembled in 19 spreadsheet workbook files of global ejecta fall pattern data files at 5° incremental launch latitudes from the equator to the north pole, provided as Supplement 4. Because only the terrestrial regime is considered here, the multiple spin rates of Dobrovolskis (1981) are not required, and greater resolution of the ejecta fall pattern data is provided for terrestrial ejecta transport analysis. The presented fall patterns were calculated for

5° launch latitude increments and include a 30° azimuth increment per Dobrovolskis (1981), a 5° elevation increment instead of the sole 45° elevation of Dobrovolskis (1981), and a 1% KE increment. Known ejecta fall sites and known source locations are listed with their associated references in spreadsheet Sheet1, with a copy provided in each workbook. Sheet1 also contains other useful references such as speed-to-%KE equivalence tables.

Combined Tool Value of SASolver and Helix with GlobePlot Utility

Figure 7 depicts various stages of orientation of an orbit plane in the inertial or nonrotating reference frame as generated automatically in the Graphics1 sheet of SASolver (Supplement 1). Figure 7A shows the ordinate reference orbit (ORO), which is the initial reference orbit (polar orbit equation) rotated about the -**Z** axis by the polar launch angle $\mathbf{nu}_A$. The ORO is then rotated about -**X** axis by the AZ to get the intermediate orbit A shown in Figure 7B. The intermediate reference orbit A is then rotated about the -**Y** axis by the launch latitude to get the intermediate orbit B shown in Figure 7C. Finally, the intermediate reference orbit B is rotated about the -**Z** axis again by launch latitude to achieve the solution orbit orientation shown in Figure 7D. The operations are order-specific. SASolver provides accounting for all of these orientations while also allowing each to be viewed with its own dedicated view angles, scaling factors, and other supporting attributes. Variable view attributes of SASolver sheet Graphics1 (i.e., Fig. 7) are helpful to tease out details of specific steps within the solution process, while uniform view attributes are useful for keeping an uninitiated audience oriented to the presented content. A student or researcher may use the SASolver Graphics1 imagery to carefully examine and present a single particular trajectory solution using variable view attributes. Faculty may prefer uniform view attributes for the four frames of Figure 7 while instructing a class of earth and planetary science students if they have never seen these tools before.

None of these intermediate orientations amounts to a new finding or big-picture significance, other than there are lots of them, and things get complicated quickly when we try to fully expand the ***A***-to-***B*** suborbital problem. Their seemingly arbitrary names may only make good test questions for rote memorization, but simply knowing of their existence is important to gain respect for the solution methodology. Ghost images of the previous or "rotated-from" orientations exist on Figure 7 panels B, C, and D. The GlobePlot utility allows consistent presentation for careful comparisons and observations. The orbit plane orientation is relative to the inertial or nonrotating frame, with inertial axes parallel to Earth's centered fixed (ECF, rotating) frame at the moment of launch. Fall point longitude calculation must account for this fact using the product of loft duration (ToF) and Earth's spin rate to get a final answer in Earth's ECF or rotating frame.

Figure 8 depicts back-solved launch solutions for the mid-elevation launch value (25° EL) for Chapman conditions of reentry mentioned in the user guide (Supplement 3) for the Central Indian Ocean (CIO) ablated button tektite specimen of Glass, Chapman, and Prasad (Glass et al., 1996). Starting at 80% Earth's escape KE, the 25° EL brown solution curve extends from ~45°S to 70°N latitude with ascribed longitude traversing only Iceland, Newfoundland, Greenland, and both Atlantic basins. The 80% KE curve is an elongate dumbbell with long N-S axis and the larger end to the north. As KE is lowered by 5% to 75% of Earth's escape KE, the shape of the solution curve collapses in N-S length and widens in E-W girth to an elongate kidney shape, still with long N-S axis, and the entire shape is translated west into the Americas.

The green 75% escape KE curve of Figure 8 is roughly evenly divided between the continental landmass of the Americas and the ocean floor. Successive 5% decreases to the blue 70% and then the purple 65% escape KE solution curves bring similar N-S contraction, with the kidney folding into its intermediate N-S zone around 12° or 13° latitude, i.e., the anti-latitude of the Central Indian Ocean button fall site of 12.6°S (and 78.5°E). The purple 65% escape KE curve begins to form an inversion cusp across Nicaragua, also at the anti-latitude of the fall point. The cusp is the transitioned length of the solution curve where launch azimuth has become outwardly directed relative to the region

Figure 7. Output of the presented suborbital solver spreadsheet SASolver includes these four sequential orientations of the orbit plane relative to Earth centered inertial (nonrotating) coordinates, the ECI frame. The set of four diagrams is lifted directly from sheet Graphics1 of the spreadsheet tool. Frame A: the ordinate reference orbit or ORO, in the equatorial plane with launch point A at 0, 0 lat/long as implied by the name. Frame B: the intermediate orbit A or IOA (ORO rotated to launch azimuth). Frame C: the intermediate orbit B or IOB (IOA rotated to launch latitude). Frame D: the solution orbit (IOB rotated to launch longitude). The high degree of detail in the four frames offers improved clarity for students and/or new users not accustomed to the suborbital paradigm or 3-D intensive rotational geometry problems, i.e., for non-astroscientists. In the programmed solution of the ***A***-to-***B*** suborbital problem, the +**X** axis intersects the prime meridian at time = 0, the moment of launch from ***A***. The Earth centered fixed coordinate (ECF) frame is coincident with the ECI frame at $t = 0$, while rotating with Earth about the +**Z** axis for $t > 0$ during time of flight (ToF). Reference latitudes are shown while continental outlines are purposefully omitted because these inertial frame images show the entire suborbital path, with no exact time defined. The shape or eccentricity ***e*** and the size or semi-major axis ***a*** of the suborbital ellipse determine the ToF from ***A*** to ***B***, allowing computation of point ***B*** or fall point longitude based on Earth's rotational rate. Trajectory data for viewing in the rotating or ECF frame in conjunction with Earth's surface details (not shown) are also computed by default within SASolver. The Graphics1 sheet is set up to be stand-alone within the SASolver spreadsheet workbook, and may also be disabled or deleted for improved throughput speed for users not interested in the graphical portion of the step-by-step methodology. Computing platforms with slow or limited graphics capacity, or macro-driven batch mode jobs in SASolver may benefit from disabling or removing sheet Graphics1.

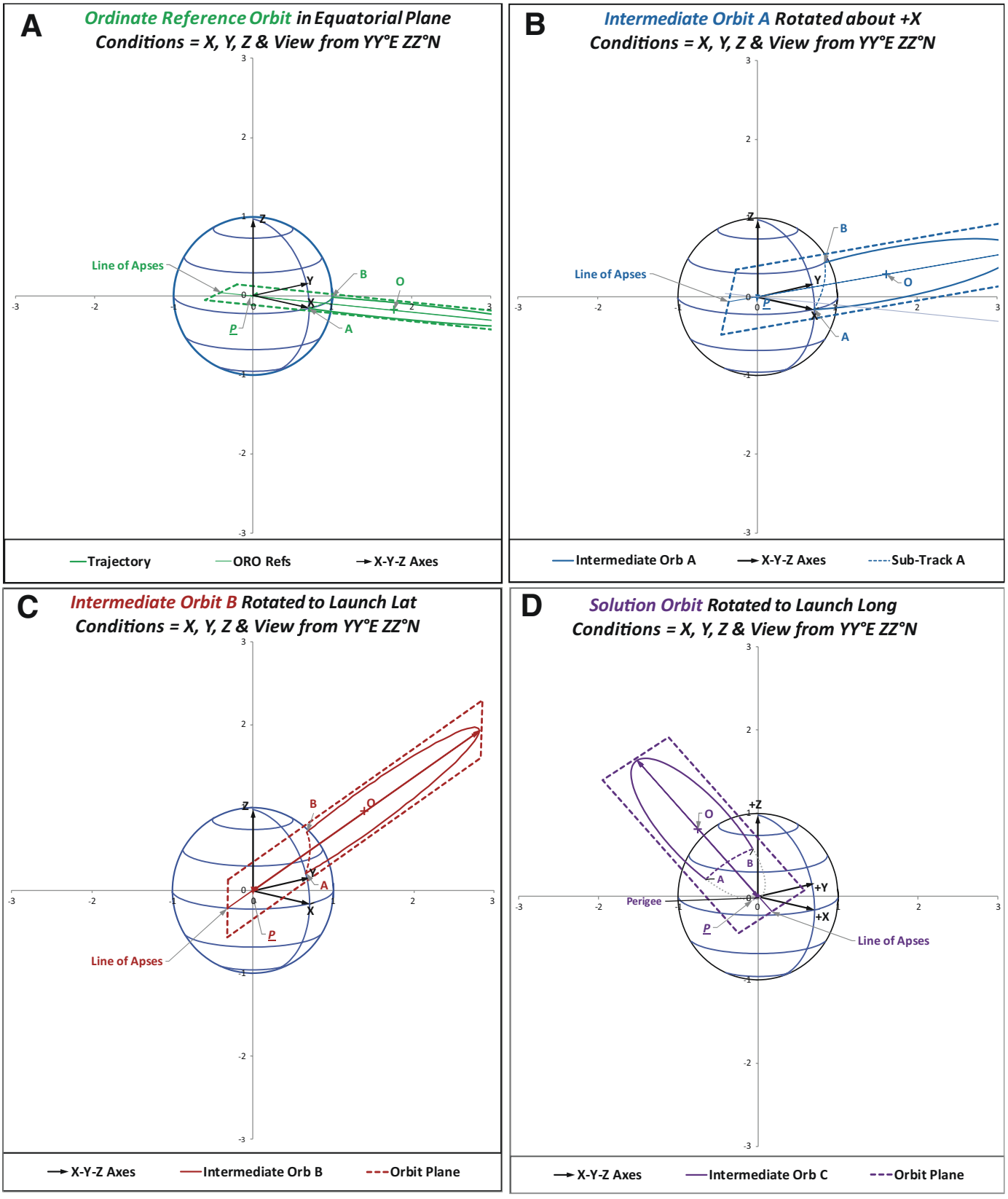

Figure 7.

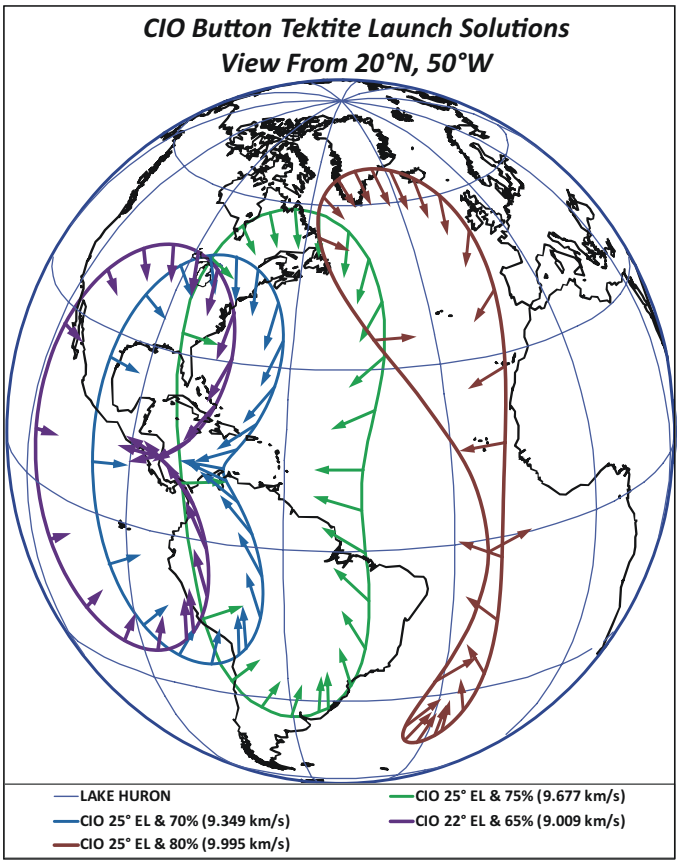

Figure 8. Back-solved launch solutions for the midelevation launch value (25° EL) for Chapman conditions of ablated button tektite reentry for the Central Indian Ocean (CIO) specimen of Glass, Chapman, and Prasad (Glass et al., 1996). These curves are the set of all launch conditions that will reach that tektite fall site given Chapman test–derived conditions of reentry for that specimen. Starting at 80% Earth's escape kinetic energy (KE), the 25° EL brown solution curve extends from ~45°S to 70°N latitude and traverses only Iceland, Newfoundland, Greenland, and both Atlantic basins in an elongate dumbbell with long N-S axis and larger end to the north. As KE is lowered by 5% to 75% of Earth's escape KE, the shape of the solution curve collapses in N-S length and widens in E-W girth to an elongate kidney shape, still with long N-S axis, and the entire shape moves west into the Americas. The green 75% escape KE curve is roughly evenly divided between the continental landmass of the Americas and ocean floor. Successive 5% decreases to the blue 70% and then the purple 65% escape KE bring similar N-S contraction of the associated solution curves, with the kidney folding into its medial N-S zone around 12° or 13° latitude, i.e., the anti-latitude of the CIO fall site of 12.6°S, 78.5°E. The CIO button tektite reentered at something less than 10 km/s, going fast enough for substantial ablation (i.e., ~ 9 km/s or more, corresponding to ~65% escape KE), albeit without any anterior face ring waves found on its S. australite ablated tektite cousins, indicating lower late stage dynamic pressure than the australites. Although Chapman wasn't sure of the CIO reentry speed other than being <10 km/s, together the 75%, 70%, and 65% KE curves share a single common crossing in the North American Great Lakes region when resolved with the presented analysis tools and governing simplified two-body gravitational model.

enclosed by the curve, after being entirely inwardly directed relative to that enclosed region for the higher-energy cases of 70%, 75%, and 80% escape KE. These qualitative features are definitive in the evolution of ***A***-to-***B*** back-solved solutions through the launch KE domain, thus their elaboration in detail. Independent efforts to work the Chapman problem will require such observational details, and perhaps other attributes as well, when describing the results for comparison.

For the Chapman problem where fall point ***B*** is known and some atmospheric reentry condition variables are known at ***B***, flight path angle may be assumed to be symmetric (equal and opposite) from launch to fall. Reentry flight path angle below horizontal at fall point ***B*** is assumed to be equal to the EL above horizontal at point ***A***. This is subject to some error, depending on the frame to which the reentry conditions are related. The high altitude of the ablation process is characterized by significant atmospheric speeds relative to Earth's solid frame beneath, for further complication. In any case, the high ablated button reentry speeds and relatively low EL angles reported by Chapman (1964) drive the frame errors to small values, displacing the solution curves only one or a few line widths, or roughly one tenth the distance between incremental 1° EL solutions. Back-solved or inverse ***A***-to-***B*** suborbital solutions, also notated ***A***-given-***B***, are just one of many important forms of output from the SA tool set.

Figure 9 shows back-solved Chapman conditions for the Bendigo high-ablation tektite (red curves) and the Central Indian Ocean button tektite (blue, green, and black curves) on the same chart. The concentric blue-green-black Central Indian Ocean button solution curves for 75% escape KE lie across Iceland, water, and landmass of the continental Americas. They cover limited longitude, and their launch azimuth domain is fully 360°. A triad of dark-red launch solution curves for the high-ablation Bendigo button at 80% escape KE is circumglobal, with a limited possible azimuth domain roughly symmetric about north. The solid-red 80% KE curve (center of the three red curves) has launch azimuth values from −58.8° AZ occurring near 102°E longitude to +52.0° AZ at roughly 5°E longitude. The dashed 25° EL solution (upper red curve) reaches azimuth extrema of −95° AZ for a swath of longitudes roughly centered around 100°E, and +65° AZ near 47°W longitude. The dotted 12° EL Bendigo solution curve (lowest red line) reaches azimuth extrema of −58.3° AZ around 107°E longitude, and +70.6° AZ near 19°W longitude. These attributes are offered for comparison, with slight variation expected from differing values of constants in the model, principally, the equivalent spherical Earth radius, 6378.145 km in this work, per B.M.W. (1971).

In Figure 9, the solid lines along the middle of the swath of each solution family represent solutions for the midvalued Chapman reentry conditions of the user guide (Supplement 3). The midvalued solutions cross at only two locations, one over the ocean and the other over the North American Great Lakes. To the right are the button tektite fall sites, the blue triangle in the Central Indian Ocean (78.5°E) and the red diamond in Australia

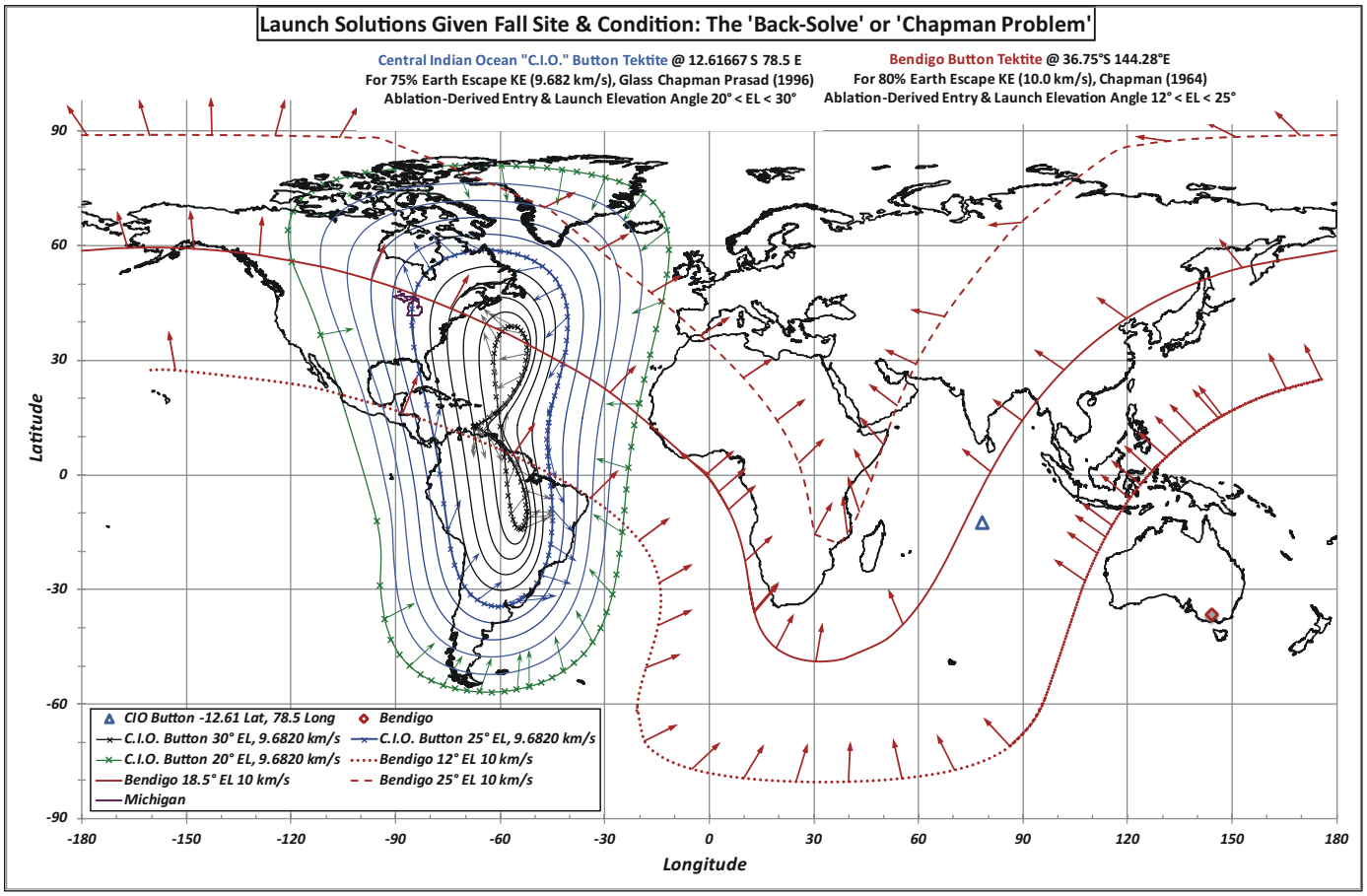

Figure 9. Back-solved solutions to the Chapman problem where fall point ***B*** is known, and two or three entry condition variables at ***B*** are known and may be assumed to be symmetric for launch point ***A*** due to suborbital symmetry. The concentric blue and green solution curves for the 75% escape kinetic energy (KE) Central Indian Ocean (CIO) button (from previous figure) tektite lie across Iceland, water, and landmass of the continental Americas. They cover limited longitude, and their launch azimuth domain is fully 360°. The dark-red solutions for the Bendigo button tektite at 80% escape KE are circumglobal. The solid-red 80% KE curve (center of the three red curves) has launch azimuth (AZ) values from −58.8° AZ occurring near 102°E longitude to +52.0° AZ at roughly 5°E. The dashed 25° elevation (EL) solution (upper red curve) reaches azimuth extrema of −95° AZ for a swath of longitudes roughly centered around 100°E longitude, and +65° AZ centered around 47°W longitude. The dotted 12° EL Bendigo solution curve (lower of the three red lines) reaches azimuth extrema of −58.3° AZ around 107°E longitude, and +70.6° AZ near 19°W longitude. The solid lines along the middle of each solution family swath represent the midvalued solution to the Chapman problem. The midvalued launch solutions for the Bendigo and CIO ablated button tektites cross twice, over the Atlantic Ocean and the North American Great Lakes. To the right are the button tektite fall sites, the blue triangle in the CIO and the red diamond in Australia, fully 4200+ km apart from each other.

(144.3°E), on the order of one full radian of central angle apart from each other, roughly one sixth of the way around the planet.

Figure 10 uses Helix and SASolver solutions to investigate the North American strewn field and associated Chesapeake impact structure. Figure 10A depicts the namesake plot from Helix, where the KE of required ***A***-to-***B*** launch conditions is considered for the Chesapeake Bay launch point ***A*** and multiple points ***B***. This is a map of the launch KE–space, or KE as a function of launch directions measured in AZ and EL, with magnitude normalized to Earth's escape KE. Figure 10A represents the data from both frames of Figure 5 for several fall locations, in a high-information-density format. Suborbital transport solution functions for the Chesapeake impact ejecta fall points tend to cluster in a tight "tree trunk," proximal to and slightly east of the **Up** vector, indicating a possible near-vertical, singular jetting solution to populate the entire strewn field. A three-view version of this is also helpful but is not shown here.

Figure 10 demonstrates that bediasites and georgiaites that launched at nearly identical conditions within the proposed jet could still fall at their observed emplacement distance ratio from the source of roughly 2-to-1. Figure 10B shows an overhead view of possible jetted trajectories directed slightly east of vertical, and their ground tracks, to populate the North American strewn field. Figure 10C depicts the scale and shape of the trajectories in Earth's rotating frame, with bediasites (Texas) and Barbados fall sites >4200 km apart, unit Earth radius scale at top, and

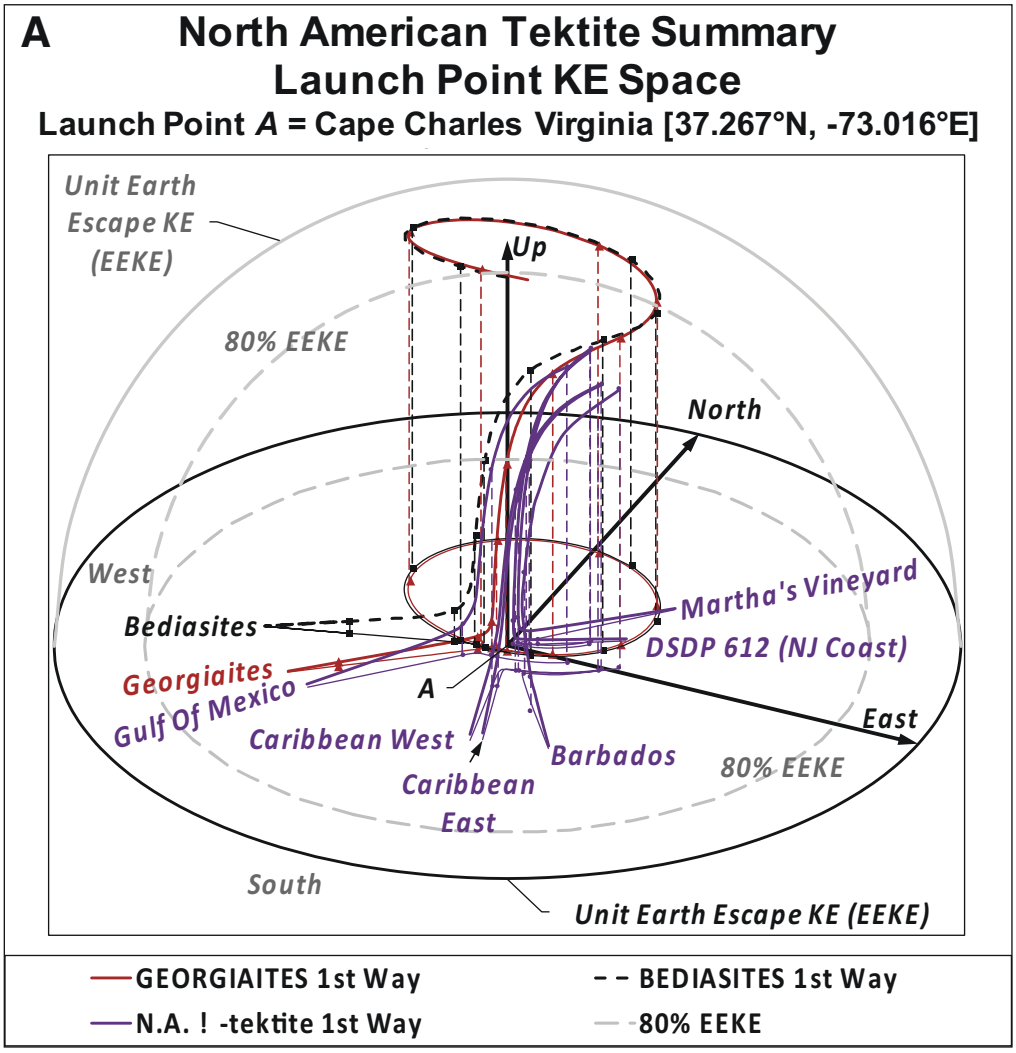

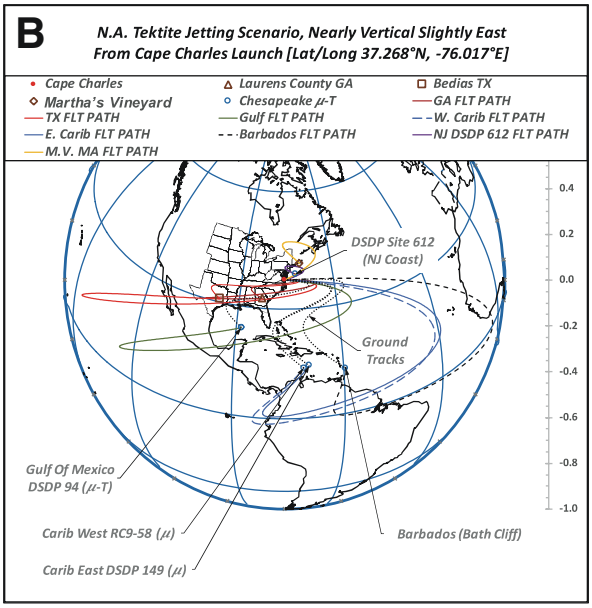

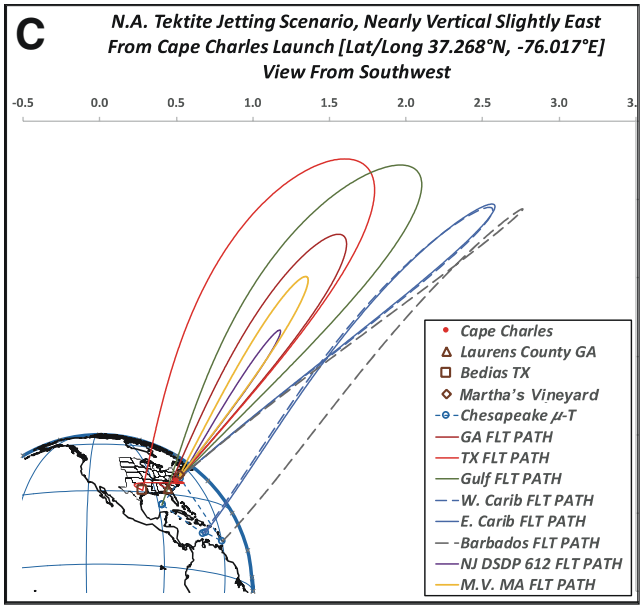

Figure 10.

Figure 10. Helix and SASolver solutions used to investigate the North American strewn field relative to the parent Chesapeake impact structure. (A) Namesake plot from Helix, where kinetic energy (KE) of required ***A***-to-***B*** launch conditions is considered for a given launch point ***A*** and multiple fall points ***B***. This is a map of the launch KE–space, or KE as a function of launch azimuth (AZ) and elevation (EL), in magnitude normalized to Earth's escape KE. Suborbital transport solution functions for the Chesapeake impact ejecta fall points tend to cluster in a tight "tree trunk" proximal to and slightly east of the ***Up*** vector, indicating a possible near-vertical, singular jetting solution to populate the entire strewn field. DSDP—Deep Sea Drilling Project; NJ—New Jersey. (B) Overhead view of possible jetted trajectories directed slightly east of vertical, and their ground tracks, to populate the North American (N.A.) strewn field. GA—Georgia; TX—Texas; μ-T—micro-tektite; MA—Massachusetts. (C) Scale and shape of the trajectories in Earth's rotating frame, with bediasites (Texas) and Barbados fall sites >4200 km apart. Such large-scale trajectories (apogee of several Earth radii) are typically not considered by geoscientist tektite researchers. This is the scale suggested by the strewn-field layout and compositional details when combined with the proper governing mechanics of suborbital ejecta transport. Devolatilized, vacuum quenched, and sometimes reentry ablated tektites have to reach the vacuum of space for some duration to acquire their imprinted features. Jetting from an impact provides mechanistic feasibility for ejecta melt transport through atmospheric breach and beyond. The presented suborbital analysis spreadsheet tools provide a means to identify and characterize such transport processes. Figure 10 suggests a practical, straightforward method where none previously existed, with the provided tools applied to information already available within the existing body of tektite research. All three panels are shown in Earth's rotating frame.

similar-scale bediasite (red), Gulf of Mexico (green), Caribbean (overlapping solid and dashed blue), and Barbados (sole dashed) fall site trajectories. Although such large-scale trajectories (apogee of several Earth radii) are typically not considered by geoscientist tektite researchers, this is the scale suggested by the strewn-field layout and compositional details when combined with the proper governing mechanics of suborbital ejecta transport. Apparently, these tektites did not get any memo on consensus procedure. All three panels are shown in Earth's rotating frame.

Further results are not required to demonstrate the diverse utility of the subject tools. SASolver and Helix spreadsheet tools, in combination with the global ejecta fall pattern data set and GlobePlot graphics utility, provide a formidable arsenal for application of suborbital analysis in the study of terrestrial ejecta ballistic transport. The scope of available results and presentation formats affords a new language, or channel of communication, among students, researchers, and instructors of terrestrial ejecta suborbital ballistic transport analysis. The results include not only single or grouped suborbital flight paths and associated ground tracks, but also comparative formats for local-frame launch kinetic energy and launch direction across many solutions between the same two ***A*** and ***B*** points, global ejecta fall patterns for any launch latitude in 5° increments and 5° launch elevation increments through a full range of launch KE from 1% to 99% of Earth's escape KE, and back-solved or "***B***-given-***A***" launch location solution functions of global layout. Because of the diversity of results, a diversity of presentation formats is also depicted and offered as native within the SA spreadsheet tool output.

CONCLUSION

The ***A***-to-***B*** suborbital model for ejecta fall emplacement on a rotating planet is coded in a pair of spreadsheet tools provided with this work. The suborbital ballistic trajectory analysis tools provide multiple forms of solution for the ***A***-to-***B*** suborbital problem. The traditional ballistic solver SASolver (Supplement 1 [see footnote 1]) determines fall point ***B*** for user-input values of launch conditions and location. A sibling spreadsheet tool calculates an extensive and diverse set of trajectories for any known ***A***-to-***B*** pair, solving the same ***A***-to-***B*** problem for multiple preset loft durations or ToF values from minimum possible value to that plus another 24 h. The helical appearance of these solution functions through full-circle azimuth prescribes the title Helix (Supplement 2). Helix solves the "all ***A***-to-***B***" problem, providing a baseline of comparison and trend space that are not easily realized with the one-at-a-time approach of SASolver alone. A third utility, GlobePlot, provides novel spherical-Earth projection plots with or without hidden lines removed at the discretion of the user. Supplement 3 contains Appendix S1 and the user guide for SASolver, Helix, and GlobePlot. Supplement 4 contains global ejecta fall pattern tables for wide-ranging launch conditions and launch location latitude.

The location of ejection or launch point ***A*** may be "back-solved" given a location for fall point ***B*** and at least two assumed launch conditions at ***A***, totaling four out of the seven variables of state. In such a solution, one of the three unknown variables is typically assumed (i.e., AZ), and the other two are iterated to resolve pairs that match the assumed value (i.e., latitude and longitude of launch point ***A***). The back-solve process of the greater ***A***-to-***B*** suborbital problem is an important technique, representing a technical challenge with extensive, detailed specifics and many pitfalls. Full treatment is beyond the present scope, while users of these tools are encouraged to give it a try. Every version of the solution is of interest in the "Chapman problem" that NASA never solved during President Kennedy's lunar mandate of the 1960s.

A-to-***B*** solution strategy may employ the one-dimensional Goal Seek function to show an answer quickly, but not necessarily the expected or desired answer. Care must always be exercised during pursuit of the SA practice that the presented tools are designed to support. Some of the seven ***A***-to-***B*** problem variables are relational instead of purely functional, and some are piecewise discontinuous, depending on regimes of the other state parameters. ToF is a preferred proxy when dealing with various arrangements of the governing mechanics per Harris (2015), because it is defined through all regimes of the suborbital

paradigm and (naturally) singular through that entire domain due to the governing Newtonian two-body orbit model. Helix makes use of this fact, producing volumes of solutions far faster than SASolver for the accustomed user, with essentially no more effort than required for SASolver. SASolver will tell you where fall point ***B*** is given launch point ***A*** and launch conditions at ***A***. Helix then expands the solution through its full possible domain within that particular ***A***-to-***B*** space. Together, they are complementary and provide the best utility for research and education.

The spreadsheet tools SASolver (Supplement 1) and Helix (Supplement 2) are designed to provide a more complete appreciation for the complex nature of the ***A***-to-***B*** suborbital problem. The output of these spreadsheet tools is sometimes humbling and confounding, which is exactly why the tools are all the more important to have available as a common reference in the public domain. The tools enable detailed consideration of the ***A***-to-***B*** suborbital paradigm for ejecta transport modeling of simple order. Atmospheric effects are neglected, and Earth is treated as spherical in the mechanical model, making it inaccurate and useless for defense application. Its precision and relative simplicity, however, provide multifaceted utility for comparative analysis of various ejecta transport trends and concepts. SASolver, Helix, and GlobePlot spreadsheet utilities, combined with the global ejecta fall pattern data set of Supplement 4, provide a formidable arsenal for application of suborbital analysis to the technical study of ballistic ejecta suborbital transport in a terrestrial setting.

ACKNOWLEDGMENTS

Acknowledgments are due to Hal Povenmire, B.P. Glass, M.E. Davias, K.A. Hilferty, P.H. Schultz, G. Herzog, M.S. Cramer, H. Burchard, P.A. Harris, N. Artemieva, and A.M. Demopolous for informative communication and *inspirational* critical comments, and to reviewers Anthony Dobrovolskis, Walter Alvarez, Thomas R. Howe III, David King, and Alvaro Suarez for valuable critical contributions. This goes especially for W. Alvarez for his verification and introspective shared experience and to T.R. Howe III for extensive combing of the spreadsheets. Thanks go to M.E. Davias for tireless supply of extensive, high-accuracy morphologic data that to any orbit analyst look clearly like 50,000+ ballistic targeting diagrams, a chilling astrodynamic signature inspiring equally tireless, extensive analysis and tool development applied to the same; it is sad that Newton and Chapman could not be here to see it. Finally, due credit goes to tireless volume editor Donna Jurdy for her brilliant reviewer recruiting and patience with this author. Without her dedicated efforts this manuscript would have died at the starting gate, and that support deserves special recognition.

REFERENCES CITED

Alvarez, W., 1990, Interdisciplinary aspects of research on impacts and mass extinctions: A personal view, *in* Sharpton, V.L., and Ward, P.D., eds., Global Catastrophes in Earth History; and Interdisciplinary Conference on Impacts, Volcanism, and Mass Mortality: Geological Society of America Special Paper 247, p. 93–97, https://doi.org/10.1130/SPE247.

Alvarez, W., 1996, Trajectories of ballistic ejecta from the Chicxulub Crater, *in* Ryder, G., Fastovsky, D.E., and Gartner, S., eds., The Cretaceous-Tertiary Event and Other Catastrophes in Earth History: Geological Society of America Special Paper 307, p. 141–150, https://doi.org/10.1130/0-8137-2307-8.141.

Bate, R.R., Mueller, D.D., and White, J.E., 1971, Fundamentals of Astrodynamics: New York, Dover Publications, 455 p.

Chapman, D.R., 1964, On the unity and origin of the Australasian tektites: Geochimica et Cosmochimica Acta, v. 28, no. 6, p. 841–880, https://doi.org/10.1016/0016-7037(64)90036-5.

Chapman, D.R., and Larson, H.K., 1963, Lunar Origin of Tektites: National Aeronautics and Space Administration (Ames Research Center) Technical Report D-1556, 66 p., https://ntrs.nasa.gov/api/citations/19630003053/downloads/19630003053.pdf.

Chapman, D.R., Larson, H.K., and Anderson, L.A., 1962, Aerodynamic Evidence Pertaining to the Entry of Tektites into the Earth's Atmosphere: National Aeronautics and Space Administration (Ames) Technical Report R-134, 24 p., https://ntrs.nasa.gov/api/citations/19630008899/downloads/19630008899.pdf.

Dobrovolskis, A., 1981, Ejecta patterns diagnostic of planetary rotations: Icarus, v. 47, no. 2, p. 203–219, https://doi.org/10.1016/0019-1035(81)90167-6.

Glass, B.P., and Koeberl, C., 2006, Australasian microtektites and associated impact ejecta in the South China Sea and the middle Pleistocene supereruption of Toba: Meteoritics & Planetary Science, v. 41, no. 2, p. 305–326, https://doi.org/10.1111/j.1945-5100.2006.tb00211.x.

Glass, B.P., Chapman, D.R., and Prasad, M.S., 1996, Ablated tektite from the Central Indian Ocean: Meteoritics & Planetary Science, v. 31, p. 365–369, https://doi.org/10.1111/j.1945-5100.1996.tb02074.x.

Harris, T.H.S., 2015, Suborbital transport mapping with time of flight (ToF), *in* Bridging the Gap III: Impact in Nature, Experiment, and Modeling Conference, University of Freiburg, Germany, September 21–26, 2015, abstract 1042.

Hayward, B.W., Kawagata, S., Sabaa, A., Grenfell, H.L., Van Kreckhoven, L., Lewandowski, K., and Thomas, E., 2012, The Last Global Extinction (Mid-Pleistocene) of Deep-Sea Benthic Foraminifera (Chrysalogoniidae, Ellipsoidinidae, Glandulonodosariidae, Plectofrondiculariidae, Pleurostomellidae, Stilostomellidae), Their Late Cretaceous–Cenozoic History and Taxonomy: Cushman Foundation for Foraminiferal Research Special Publication 43, 408 p.

Schultz, P.H., and Gault, D.E., 1990, Prolonged global catastrophe from oblique impact, *in* Sharpton, V.L, and Ward, P.D., eds., Global Catastrophes in Earth History; An Interdisciplinary Conference on Impacts, Volcanism, and Mass Mortality: Geological Society of America Special Paper 247, p. 239–262, https://doi.org/10.1130/SPE247-p239.

Stauffer, P.H., 1978, Anatomy of the Australasian tektite strewnfield and the probable site of its source crater, *in* Nutalay, P., ed., Proceedings of the 3rd Regional Conference on the Geology and Mineral Resources of Southeast Asia: Bangkok, Thailand, Asian Institute of Technology, the Canadian International Development Agency and the Geological Society of Thailand, p. 285–292.

Manuscript Accepted by the Society 1 June 2021
Manuscript Published Online 7 March 2022

Printed in the USA